

JGR Atmospheres

RESEARCH ARTICLE

10.1029/2020JD033538

Special Section:

Carbon Weather: Toward the next generation of regional greenhouse gas inversion systems

Key Points:

- A severe haze pollution at the leading edge of a cold front in China on December 9, 2016 is examined using multisensors and multimodels, including WRF-Chem and WRF-CO₂
- Satellite-retrieved column-averaged CO₂ data can be used to monitor air pollution events collectively with other in-situ and remote-sensing instruments
- Channel winds between Mountains Dabie and Huang transport pollutants from the North China Plain and Yangtze River Delta Region to Jiangxi province

Supporting Information:

Supporting Information may be found in the online version of this article.

Correspondence to:

X.-M. Hu,
xhu@ou.edu

Citation:

Hu, X.-M., Hu, J., Gao, L., Cai, C., Jiang, Y., Xue, M., et al. (2021). Multisensor and multimodel monitoring and investigation of a wintertime air pollution event ahead of a cold front over eastern China. *Journal of Geophysical Research: Atmospheres*, 126, e2020JD033538. <https://doi.org/10.1029/2020JD033538>

Received 15 JUL 2020
Accepted 29 APR 2021

Author Contributions:

Conceptualization: Changjie Cai
Data curation: Yujun Jiang
Formal analysis: Jun Hu, Lan Gao
Funding acquisition: Ming Xue
Methodology: Tianliang Zhao
Writing – review & editing: Sean M. R. Crowell

© 2021, American Geophysical Union.
All Rights Reserved.

Multisensor and Multimodel Monitoring and Investigation of a Wintertime Air Pollution Event Ahead of a Cold Front Over Eastern China

Xiao-Ming Hu¹ , Jun Hu^{1,2}, Lan Gao³, Changjie Cai⁴, Yujun Jiang⁵, Ming Xue¹ , Tianliang Zhao² , and Sean M. R. Crowell⁶ 

¹Center for Analysis and Prediction of Storms, University of Oklahoma, Norman, OK, USA, ²Collaborative Innovation Center on Forecast and Evaluation of Meteorological Disasters, Key Laboratory for Aerosol-Cloud-Precipitation of China Meteorological Administration, Nanjing University of Information Science and Technology, Nanjing, China,

³School of Meteorology, University of Oklahoma, Norman, OK, USA, ⁴Department of Occupational and Environmental Health, University of Oklahoma Health Sciences Center, University of Oklahoma, Oklahoma City, OK, USA, ⁵Zhejiang Lin'an Atmospheric Background National Observation and Research Station, Hangzhou, China, ⁶GeoCarb Mission, University of Oklahoma, Norman, OK, USA

Abstract Given the limitations in pollutant measurements (e.g., coverage, observation errors) and air quality model uncertainties (e.g., with parameterizations and emissions), a multisensor and multimodel approach offers additional benefits compared to a single-instrument and deterministic approach for monitoring, investigating, and predicting air pollution events. In this study, we use multisensors (including the spaceborne MODIS, OCO-2, AIRS, and OMPS instruments as well as surface instruments) and multimodels (including WRF-Chem and WRF-CO₂) to investigate a severe air pollution event on December 9, 2016 over eastern China. During this episode, a strong cold front moved southward. At the leading edge of the front, WRF-CO₂ simulates an enhanced XCO₂ belt while WRF-Chem simulates a belt of high PM_{2.5} concentration. The XCO₂ and PM_{2.5} belts are generally colocated, due to coemission of CO₂ and pollutants (or their precursors). Satellite observations including MODIS AOD, OCO-2 XCO₂, OMPS NO₂, AIRS CO, and surface data confirm the simulated pollution and XCO₂ belts. Later on, the front became distorted due to terrain blocking and mountain channel flows. Both observations and simulations show that the channel winds between Mountains Dabie and Huang transport the haze plume into Jiangxi province, enhancing pollution in the region. It is concluded that the multisensor (including space-based and ground-based instruments) and multimodel (e.g., WRF-CO₂, WRF-Chem) approach can be used to collectively monitor and investigate air pollution events, given that emissions of the involved species have generally similar spatial distributions.

1. Introduction

Severe air pollution continues to plague a few regions around the world, e.g., China and India (Fu & Li, 2020; Guo et al., 2019; Krotkov et al., 2016; Li et al., 2017; Wang & Hao, 2012), with most haze pollution events occurring in winter and late fall (Li, Hu, Ma, et al., 2019; Li, Hu, Shi, et al., 2019; Miao et al., 2015). Various instruments (including both in-situ and remote sensors) and numerical models are used to monitor and examine air quality (e.g., Ding et al., 2013; Ji et al., 2014; Sun et al., 2015; Wang, Wei, et al., 2014; Wang, Li, et al., 2014). Serving as a numerical laboratory and integrating our knowledge on how physical and chemical processes affect pollutant concentrations, the grid-based Eulerian models are widely used to investigate air pollution (Russell, 1997); however, the uncertainties within the model simulations cannot be overlooked. Given model errors/uncertainties associated with both meteorological and chemical processes/inputs, substantial uncertainties of a single deterministic simulation with one air quality model are always of concern when examining impact of emission abatement (Leibensperger et al., 2011), climate change effects (Tai et al., 2012), aerosol radiative effects (Gao et al., 2020), health and agriculture impacts of air pollution (Ahmadov et al., 2007), regional to continental transport (Dong et al., 2018; Galmarini et al., 2017), as well as conducting air quality forecasting (Hu, 2015; Li, J., Nagashima, et al., 2019). A multi-model approach instead has been shown more beneficial to investigate these air pollution issues, which can constitute an envelope of realizations of the scenario that adequately represents our understanding of the

processes involved (Colette et al., 2011, 2012, 2017; Fiore et al., 2009; Kim et al., 2019; Sokhi et al., 2008; Tai et al., 2012). These multimodel investigations (e.g., Liu et al., 2018; Ma et al., 2019; Solazzo et al., 2017) use a variety of air quality models, including the Community Multiscale Air Quality (CMAQ) Modeling System (Binkowski & Roselle, 2003; Byun & Schere, 2006), and Comprehensive Air quality Model with extensions (CAMx), which are commonly used by the U.S. Environmental Protection Agency (EPA) and other planning organizations for formulating emission control strategies. For air quality simulations in China, as other regions in the world, the primary uncertainties stem from emission inputs (Bouarar et al., 2019; Chen, Liu, Ban, et al., 2019; Kong et al., 2020; Zhao et al., 2019), as well as physical/chemical schemes (Hu et al., 2008; Li, Wang, et al., 2019). Uncertainties of emissions of certain species (e.g., CO, NH₃) in China reach as large as a factor of 2 (Kong, Tang, et al., 2019; Lu et al., 2019) and even larger at certain regions (Kong, Lin, et al., 2019). Given the large model uncertainties, a multimodel approach is desirable for examining air quality issues, as well as monitoring and predicting air pollution in China.

Complementing numerical model simulations and conventional surface in-situ measurements, satellite retrievals of pollutants, such as aerosol optical depth (AOD) from the Moderate Resolution Imaging Spectroradiometer (MODIS) (Donkelaar et al., 2010; Ma et al., 2016; Wei et al., 2019; Xie et al., 2019; Xu, Han, et al., 2019; Yu et al., 2008), Ozone (O₃) from the Tropospheric Emission Spectrometer (TES) and the Ozone Monitoring Instrument (OMI) (Zhang et al., 2010), CO from the Atmospheric Infrared Sounder (AIRS), and Measurements of Pollution in the Troposphere (MOPITT) sensors (Kopacz et al., 2010; Lowry et al., 2016; Yurganov et al., 2008), NO₂ from the Ozone Mapping Profiler Suite (OMPS) (Lin et al., 2019; Yang et al., 2014), play an important role in air quality monitoring, prediction, and inversion.

Pollutants (or their precursors) and carbon dioxide (CO₂, a primary greenhouse gas) are often coemitted and their colocated mixing ratios (as well as their spatiotemporal variations) often show a linear relationship, e.g., between CO and CO₂, and between nitrogen oxides (NO_y) and CO₂ (Brioude et al., 2012, 2013; Konakov et al., 2014; Lindenmaier et al., 2014; Reuter et al., 2019; Turnbull et al., 2011; Wunch et al., 2009; Yang et al., 2019). The linear relationship between those coemitted species has been used in many atmospheric chemistry studies, including constraining one species' emissions given observations of the other species (Brioude et al., 2012; Palmer et al., 2006; Wang et al., 2009). The relationship between CO₂ and haze pollution at regional to urban scales, however, is not examined to our best knowledge.

Anthropogenic CO₂ emissions, including fossil fuel burning and net land use change (Ciais et al., 2014), contribute significantly to global carbon budget. While fossil fuel CO₂ (FFCO₂) emissions at national scales are generally well constrained with uncertainties of 5–20% ($\pm 4\%$ for USA), uncertainties of FFCO₂ emissions at urban scales are larger (Andres et al., 2014; Gurney et al., 2019; Oda et al., 2019). Given the sparseness of surface CO₂ observations, particularly in urban areas, carbon-observing satellites provide valuable information of spatial distribution of column-averaged dry air mole fractions of CO₂ (XCO₂), which can be used to constrain anthropogenic CO₂ emissions. A few CO₂ satellites have been launched, including the Japanese Greenhouse gases Observing SATellite (GOSAT, Yokota et al., 2009) in orbit 2009, and NASA's Orbiting Carbon Observatory-2 (OCO-2, Crisp et al., 2004, 2008, 2017) in orbit 2014. When overpassing urban areas, satellite XCO₂ data can capture urban CO₂ plumes (Wu et al., 2018, 2020; Ye et al., 2020), and also more remote power plants (Nassar et al., 2017). Wu et al. (2018) carried out inverse modeling using a Lagrangian model together with OCO-2 XCO₂ data to quantify CO₂ emissions from Riyadh. Ye et al. (2020) used OCO-2 XCO₂ data, together with a Eulerian atmospheric transport model (i.e., the Weather Research and Forecasting (WRF) model), to constrain FFCO₂ emissions from four urban areas, including Riyadh (Saudi Arabia), Cairo (Egypt), Los Angeles (USA), and the Pearl River Delta metropolitan region in China. Despite these exemplary studies using satellite XCO₂ data to derive urban plume of greenhouse gases (Wu et al., 2018; Ye et al., 2020), the applications of satellite XCO₂ data for air quality purpose are not explored to the best of our knowledge.

Research of haze pollution in China mostly focused on a few most severe regions, including the north China Plains (Hu, Ma, et al., 2014, 2016), Yangtze River Delta Region (Hu, J., Li, et al., 2018; Huang et al., 2020; Li, Wang, et al., 2019; Xu, Tie, et al., 2019), Pearl River Delta region (Li et al., 2018), Sichuan Basin (Jia et al., 2019; Ning et al., 2019; Zhou et al., 2019), and northeast China (Li, Hu, Ma, et al., 2019; Li, Hu, Shi, et al., 2019). Jiangxi province, located between the Yangtze River and Pearl River Delta region and connected with Anhui province through the channel between Mountains Dabie and Huang (Figure 1), has not

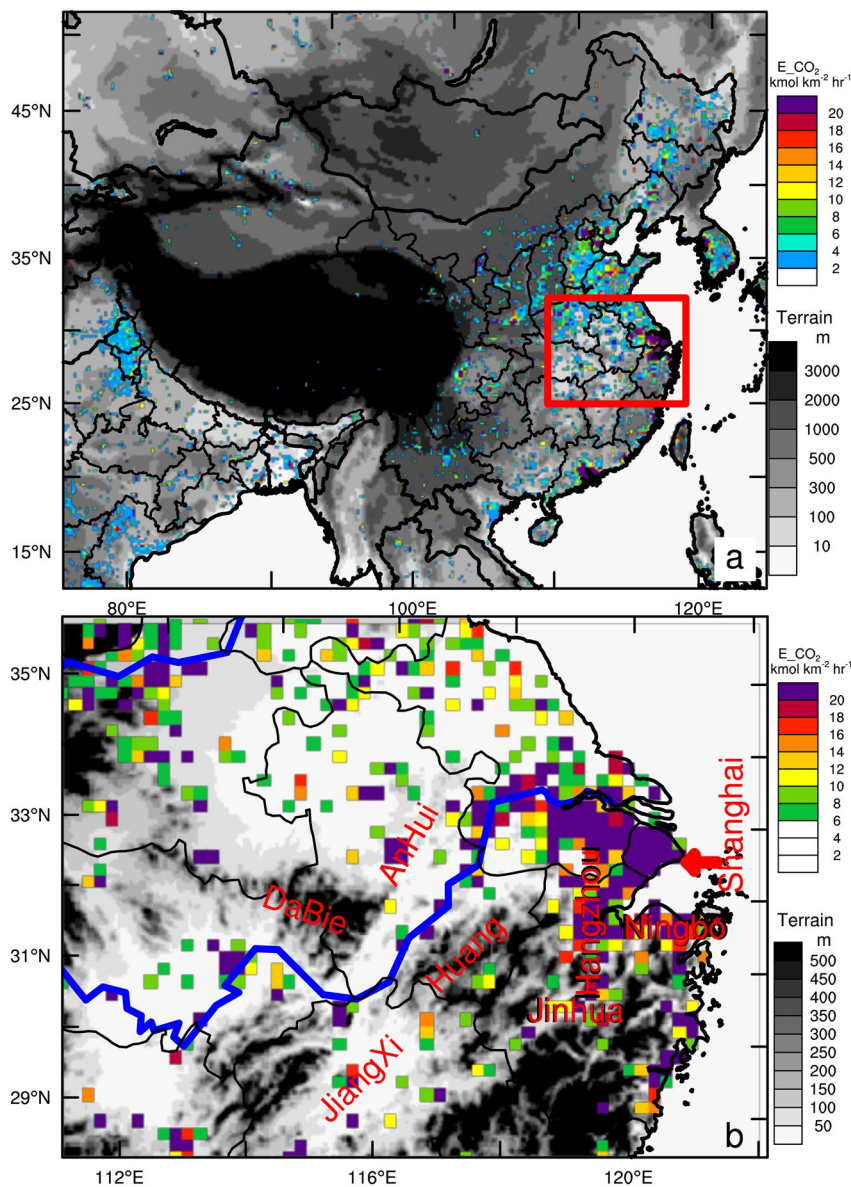


Figure 1. Domain configuration and anthropogenic CO₂ emission in (a) the first domain and (b) the second domain with relevant locations marked. The Yangtze river is marked with a blue line.

received much attention in air quality studies (Li et al., 2018; Zhao et al., 2017). As the air pollution exacerbated in recent years in the region, particularly in its capital city, Nanchang with more than 5 million residents, more investigation of its source of pollution is warranted (Liao et al., 2015; Zhang, Yuan, et al., 2014). While limited studies focused on local sources of pollution in Jiangxi province, including vehicles, industries, waste burning, and dust (Yang et al., 2017; Zhao et al., 2017), contribution from regional transport was not previously studied in detail.

Using surface in-situ observations and model simulations with the WRF model with Chemistry (WRF-Chem), Li, Wang, et al. (2019) investigated the worst haze pollution in China in 2016 occurred over the North China Plains and Yangtze River Delta Region during December 2–8, which was found to be caused by poor dispersion condition and prominent formation of secondary inorganic aerosols. The severe haze pollution (with a PM_{2.5} concentration of ~200 µg m⁻³) actually persisted until early morning on December 9 at Shanghai and late afternoon at Hangzhou (see the relevant locations marked in Figure 1b). The late

persistence of this severe haze pollution and its dissipation, as well as its impact on surrounding regions such as Jiangxi province, were not discussed by Li, Wang, et al. (2019).

In this study, the severe haze event on December 9, 2016 over eastern China is examined using a multimodel and multisensor approach, utilizing simulations with the WRF-Chem and WRF-CO₂ systems, and observations from surface sites, as well as AOD from MODIS, XCO₂ from OCO-2, NO₂ from OMPS, and CO from AIRS. The purpose of this study is to demonstrate that using such a multimodel and multisensor approach, we can better monitor, and predict air pollution events, particularly with additional information of CO₂. We will illustrate, for the first time, OCO-2 XCO₂ data and WRF-CO₂ simulations can be used to help monitor/assess/predict haze pollution, particularly in terms of its spatial distribution. We will also highlight the importance of regional transport on the pollution formation in eastern China, while detailed atmospheric chemistry is not the focus of this study. In the latter case, models with specialty in air chemistry such as CMAQ and CAMx may be more desired. In this study, the WRF-Chem and the WRF-CO₂ system are adequate and used for the objectives described above.

The rest of this paper is organized as follows. Section 2 describes the selected air pollution episode, observations, and design of WRF-Chem and WRF-CO₂ simulations. Section 3 examines the air pollution event using the two model simulations and various observations. Section 4 discusses caveats of using satellite XCO₂ data to help monitor air pollution. Conclusions are summarized in Section 5.

2. Data and Methods

2.1. Episode and Observational Data

The worst haze pollution in China in 2016 occurred over the North China Plains and Yangtze River Delta Region during December 2–9. While Li et al. (2019) focused on the formation mechanism of this haze pollution between December 2 and 8, this study will focus on the late persistence of this severe haze pollution and its dissipation, as well as its impact on surrounding region such as Jiangxi province on December 9. On December 8, a surface cold front accompanied by an upper trough approached the North China Plain (Figure S1 in Supporting Information). The cold and dry airmass behind the cold front (identified in Figure 2 from negative temperature change, positive pressure change, low dew point) kept pushing southward and affected the air quality over eastern China on December 9, 2016.

In addition to the surface in-situ measurements at the national air quality monitoring sites (Hu, Wang, et al., 2014; Zhang et al., 2015) and a regional atmospheric background station in Lin'an, Hangzhou (30.30°N, 119.75°E) (recording CO₂ and pollutants), satellite remote-sensing data are used to monitor this pollution event, including AOD from MODIS, NO₂ from OMPS, CO from AIRS, as well as XCO₂ from OCO-2 (Table 1). The OCO-2 satellite (Eldering et al., 2017) was launched in 2014, and has been collecting data since then in a sun-synchronous orbit with a local overpass solar time of about 1:30 PM. OCO-2 measures reflected sunlight in three bands, and the resultant spectra are used to infer XCO₂. The data are bias corrected and filtered using ancillary retrieved parameters (Wunch et al., 2017). In this work, we utilize the OCO-2 Version 9r (Kiel et al., 2019, retrieved from <https://co2.jpl.nasa.gov/#mission=OCO-2>). The random errors of XCO₂ data are ~0.4 ppmv evaluated against a primary ground-based validation network (Eldering et al., 2017; O'Dell et al., 2018). The high measurement precision of the OCO-2 XCO₂ data allows detection of urban CO₂ plumes (Wu et al., 2018, 2020; Ye et al., 2020).

In addition to CO₂, other pollutants (aerosol particles, CO, NO₂), measured from a series of sun-synchronous polar-orbiting satellites, are used to characterize the spatial distribution of this pollution event. AOD product from the MODIS instrument on the Aqua satellite is used in this study. Specifically, we utilize the level 2 collection 6 AOD retrieval at 550-nm wavelength over land with nadir spatial resolution of 3 km (available from <https://ladsweb.modaps.eosdis.nasa.gov/>). The 3-km product applies the similar Dark Target algorithm to the standard MODIS 10-km resolution product (Remer et al., 2013) but captures aerosol spatial gradients on a fine-scale, which is needed for air quality research (Munchak et al., 2013). Although artificially high AOD can be found from 3-km product over bright or urban surface (Remer et al., 2013), previous studies show good agreement between MODIS 3-km good quality AOD and AErosol RObotic NETwork (AERONET) AOD in eastern China (Gupta et al., 2018; He et al., 2017). Therefore, only good quality retrievals from MODIS 3-km product are included in the following analysis.

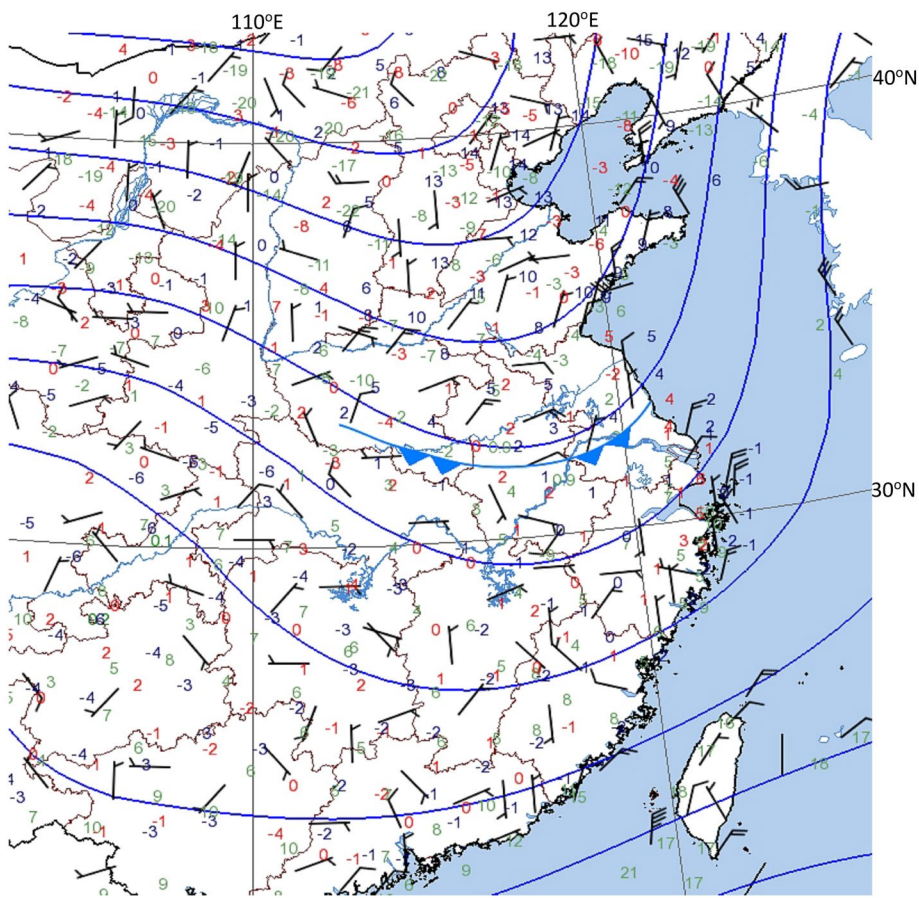


Figure 2. Surface weather maps at 0800 local time on December 9, 2016 based on observation data archived in the Meteorological Information Comprehensive Analysis and Process (MICAPS) system operated by China Meteorological Administration. The blue lines are isobars. Red, blue, and green numbers represent temperature change, pressure change in the past 24 h, and dew point.

The CO vertical column density retrieval from the Atmospheric InfraRed Sounder (AIRS) instrument on the Aqua satellite is also investigated. AIRS retrieves CO by observing thermal emission around the 4.7 μm vibrational fundamental band (Susskind et al., 2003). The instrument has a spatial resolution of 13.5×13.5 km, but the reported data are degraded to 45×45 km due to the cloud-clearing processes used in the retrieval algorithm, which can significantly increase the spatial coverage (Susskind et al., 2003). The AIRS level 2 version 6 retrieval product, which includes vertical profiles of CO, is used in this study and can

be obtained from Goddard Earth Sciences Data and Information Center (GES-DISC, <https://disc.gsfc.nasa.gov/>). The thermal-infrared measurement from AIRS yields a CO vertical sensitivity broadly peaking in the midtroposphere (300–700 mb) (Warner et al., 2007; Worden et al., 2013). In this study, only CO retrievals from the midtroposphere (500-mb layer) are considered due to the strong vertical sensitivity of AIRS CO retrievals at this level, as suggested by the AIRS team for air quality assessment (personal communication, 2020). As a consequence, a limitation in the application of AIRS CO retrievals is that some variations in the retrieved CO (e.g., moderately different from surface CO distribution) can be associated with the nonuniform vertical distribution of the CO abundance.

Table 1
List of the Four Satellite Data Used in This Study

Pollutant/species	Instrument/satellite	Product	Spatial resolution (km \times km)
CO ₂	Spectrometer/OCO-2	Level 2 version 9r	2.25×1.29
AOD ₅₅₀	MODIS/Aqua	Level 2 collection 6	3×3
CO	AIRS/Aqua	Level 2 version 6	45×45
NO ₂	OMPS/SNPP	Level 2	50×50

Note. All of them have a local overpassing time of \sim 1:30 PM. MODIS product can be found from <https://ladsweb.modaps.eosdis.nasa.gov/>. All other products can be found from <https://disc.gsfc.nasa.gov/>.

The NO₂ data used in this study are from the Ozone Mapping Profiler Suite (OMPS) Nadir Mapper onboard the Suomi National Polar Partnership (SNPP) satellite with a local ascending equator crossing time at

1:30 PM. The OMPS is a hyperspectral UV spectrometer measuring backscattered UV radiance spectra from 300-nm to 380-nm wavelength, providing daily global coverage with a nadir pixel size of 50×50 km (Yang et al., 2013, 2014). The amount of total column NO₂ can be first estimated by using a direct vertical column fitting algorithm, and the stratospheric and tropospheric amounts can be further separated by applying a new spatial technique (Yang et al., 2014). In this study, we utilize the OMPS Nadir Mapper level 2 product of tropospheric NO₂ amount. Only those pixels marked as good quality and the corresponding cloud fraction <30% are included in the analysis. The OMPS product has recently been used to investigate the NO₂ trend in China and agrees well with the measurement from Ozone Monitoring Instrument (OMI) onboard another sun-synchronous orbit satellite (Lin et al., 2019).

2.2. Air Quality Simulation With WRF-Chem

The WRF-Chem (Fast et al., 2006; Grell et al., 2005; Skamarock & Klemp, 2008) version 3.8.1 is employed for air quality simulation in this study. Two one-way nested domains are used with a 20-km grid spacing in the first domain over China and a 4-km grid spacing in the second domain focusing on eastern China (Figure 1). Forty-eight vertical layers extend from the surface to 10 hPa. The WRF-Chem simulation period spans from December 6 to 11, 2016 with hourly model outputs. The NCEP Final Global Forecast System Operational Analysis (FNL) data are used to provide the initial and boundary conditions of meteorological variables. The chemical initial and lateral boundary conditions are extracted from the global chemical transport Model for Ozone And Related chemical Tracers (MOZART) (Emmons et al., 2010; Horowitz et al., 2003). The Multiresolution Emission Inventory for China (MEIC) (<http://www.meicmodel.org/>) of December 2016 is applied for the anthropogenic emissions. The MEIC only has single layer monthly mean emission information, thus does not have vertical distribution or diurnal variation of the emissions. When preparing hourly emissions for WRF-Chem, MEIC emissions are vertically distributed in the boundary layer and a diurnal variation profile is applied following previous studies (Chen, Zhu, et al., 2019; Zhang et al., 2018). Biogenic emissions are generated online by the Model of Emissions of Gas and Aerosols from Nature (MEGAN) (Guenther et al., 2006). The physical parameterizations include the Noah land-surface model (Tewari et al., 2004), Mesoscale Model (MM5) similarity surface layer, Yonsei University (YSU) planetary boundary layer (PBL) scheme (Hong et al., 2006), RRTMG shortwave and longwave radiation schemes (Iacono et al., 2008), Morrison double-moment microphysics scheme (Morrison et al., 2009), and new Grell cumulus parameterization (Grell & Dévényi, 2002). The CBMZ gas-phase chemical mechanism (Fast et al., 2006) combined with the MADE/SORGAM aerosol model (Ackermann et al., 1998; Schell et al., 2001) is employed to represent atmospheric chemistry.

2.3. CO₂ Simulations With the WRF-CO₂ System

In 2007, an online CO₂ simulation system was developed within the WRF model framework (referred to as the WRF-CO₂ system hereafter), considering both anthropogenic CO₂ emissions and biospheric CO₂ fluxes and their subsequent atmospheric transport/dispersion (Ahmadov et al., 2007). In this system, biogenic CO₂ fluxes are calculated online using the Vegetation Photosynthesis and Respiration Model (VPRM) (Mahadevan et al., 2008; Xiao et al., 2004). In the past few years, this WRF-CO₂ system has been further developed by coupling with the CarbonTracker global simulation (Peters et al., 2007, with updates documented at <http://carbontracker.noaa.gov>) and incorporating optimized VPRM parameters (Hu, Zhang, et al., 2018, 2020, 2021). Simulation with this WRF-CO₂ system was previously used to investigate regional transport during an air pollution event in northeast China (Li, Hu, Ma, et al., 2019), given the similar spatial distribution of anthropogenic emissions of CO₂ and pollutants (Figure 3).

By using a multimodel approach to investigate the air pollution event on December 9, 2016, we try to derive the most common and robust information of this event in presence of current plausible model uncertainties. If using the same model configuration in each model, the spread of predicted meteorology and the subsequent species/pollutants would be small, which might lead to a smaller model spread comparing to model errors, an undesired outcome for ensemble/multimodel investigation. In contrast, in an ensemble forecasting practice, the use of multiple models/physics may better sample the uncertainty space (not all physics are biased in the same direction, Thomas et al., 2019) so that ensemble simulations offer more accurate/less uncertain solution. Thus, we do not intent to use the same configuration for both WRF-Chem

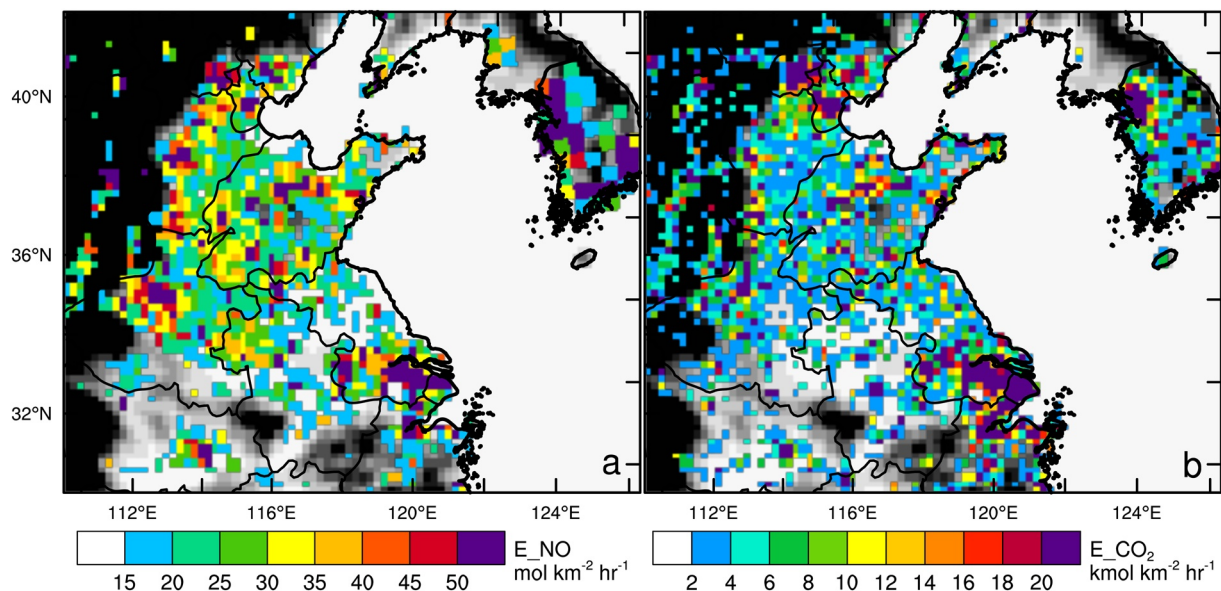


Figure 3. Spatial distribution of (a) NO emission used by the WRF-Chem simulation and (b) CO₂ emission used by the WRF-CO₂ simulation. Note that pollutant emissions over China are derived from the Multiresolution Emission Inventory for China (MEIC) (<http://www.meicmodel.org/>) and emissions outside of China are derived from Hu, Ma, et al., 2014. CO₂ emissions are derived from the Open-Data Inventory for Anthropogenic Carbon dioxide (ODIAC).

and WRF-CO₂ simulations, but only ensure selecting a likely used configuration. The WRF-CO₂ simulation conducted in this work follows a similar configuration used by our previous studies (Hu et al., 2020; Li, Hu, Ma, et al., 2019, 2020), but applying over a different domain configuration in this study (a 20-km grid spacing in the first domain and a 4-km grid spacing in the second domain, Figure 1, same as WRF-Chem). Different from the WRF-Chem simulation, which spans for the selected pollution episode, the WRF-CO₂ simulation is only a segment of a yearly downscaling simulation that uses spectral nudging to maintain the large scale forcing in the simulation domain (see Hu et al. (2020) and Li et al. (2020) for details). Thus, the CO₂ simulation for the selected December 9 episode has been spun-up for 11 months. The NCEP/DOE R2 data (Kanamitsu et al., 2002) provide meteorological initial and boundary conditions and the CarbonTracker global simulation (version CT2017) $3^\circ \times 2^\circ$ outputs (Peters et al., 2007) provide CO₂ initial and boundary conditions. Since the investigated period is in winter, biogenic CO₂ fluxes are minor and the spatiotemporal variation of CO₂ mixing ratios are dominated by anthropogenic CO₂ emissions and the subsequent transport and dispersion. The monthly $0.1^\circ \times 0.1^\circ$ Open-Data Inventory for Anthropogenic Carbon dioxide (ODIAC) (Oda et al., 2018, 2019) version 2018 (Figure 1) provides the anthropogenic CO₂ emission. Since lack of height information of the emissions, all the ODIAC CO₂ emission is put at the first model layer. ODIAC was prepared integrating a few data sources, including Carbon Dioxide Information Analysis Center (CDIAC) global and national fossil fuel emission estimates, BP statistical review of world energy, power plants geolocation information from the Carbon Monitoring and Action (CARMA) global power plant database, and satellite observed nightlight data (Lauvaux et al., 2016; Oda et al., 2019). ODIAC has been widely used in CO₂ studies in recent years (Hedelius et al., 2018; Hu et al., 2020; Lauvaux et al., 2016; Martin et al., 2019; Oda et al., 2017; Ye et al., 2020). Oceanic CO₂ fluxes are taken from climatological monthly values derived by Takahashi et al. (2009). The oceanic contribution to total CO₂ concentration is negligible (Hu et al., 2020) comparing to the dominant anthropogenic contribution in this study.

Major model physics parameterizations selected for the WRF-CO₂ simulation include the Dudhia shortwave radiation scheme (Dudhia, 1989), the rapid radiative transfer model (RRTM) (Mlawer et al., 1997) for long-wave radiation, the Noah land-surface model (Chen & Dudhia, 2001), the Grell-3 cumulus scheme (Grell & Dévényi, 2002), the Morrison microphysics scheme (Morrison et al., 2009), and the YSU PBL scheme (Hong et al., 2006).

Two additional single-domain short WRF-CO₂ simulations are conducted with turning on/off anthropogenic CO₂ emissions over the North China Plain (NCP, north of 34°N) for the December 6–9 episode, in order to

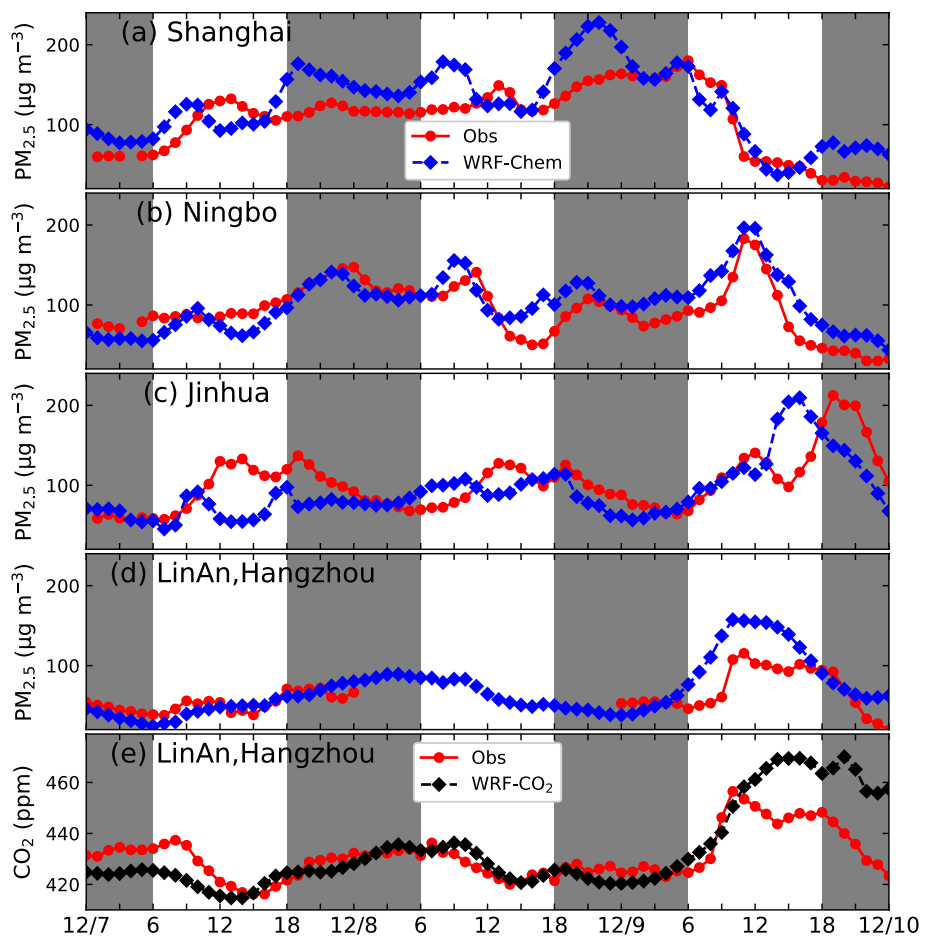


Figure 4. Time series of PM_{2.5} at four sites in the Yangtze River Delta Region, (a) Shanghai, (b) Ningbo, (c) Jinhua, and (d) LinAn, Hangzhou (see their locations in Figure 1(b)), and (e) CO₂ at LinAn, Hangzhou. Nighttime is shaded.

quantitatively estimate the contribution of regional transport of NCP emissions to pollution in the middle and lower reaches of the Yangtze River region.

3. Results

Li, Wang, et al. (2019) investigated the haze pollution over eastern China during December 2–8, 2016 and briefly mentioned that on the last two days of this episode, i.e., on December 7–8, the air pollution in the region experienced the rapid formation and dissipation stages. The severe haze pollution (with a PM_{2.5} concentration of ~200 µg m⁻³) actually persisted until December 9 in the Yangtze River Delta Region, e.g., until early morning at Shanghai, noon at Ningbo/Hangzhou, and late afternoon at Jinhua (Figures 4a–4d). Meanwhile, a surface CO₂ site in the region, at Linan, Hangzhou recorded an elevated CO₂ concentration (Figure 4e).

The PM_{2.5} peak gradually delayed at sites from north to south in eastern China on December 8–9, 2016 (Figure 4), consistent with the southward movement of a frontal system. On December 9, a trough at 850 hPa moved off the coast of northeast China and the northwesterly wind dominated over northeast China and North China Plains (Figure S1 in Supporting Information). Correspondingly, at surface the high-pressure system with a cold front at the leading edge penetrated over the North China Plains and Yangtze River Delta Region, and northerly surface winds persisted in the region (Figure 2).

Both models (WRF-Chem and WRF-CO₂) reproduce the southward penetration of the cold front (Figures 5 and 6) and simulate elevated PM_{2.5} and XCO₂ concentrations at the leading edge of the front (Figures 5b, 5c,

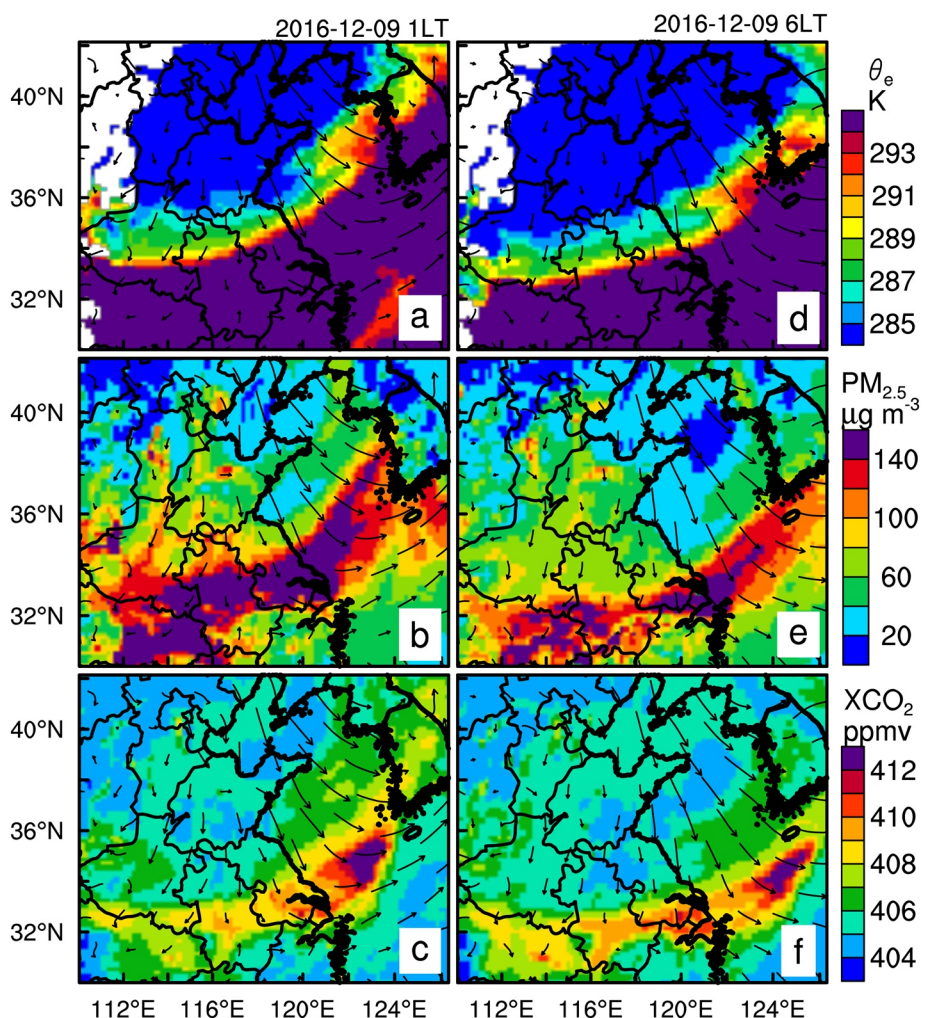


Figure 5. Simulated (a, d) equivalent potential temperature (θ_e) at 1 km above sea level, (b, e) surface $\text{PM}_{2.5}$ by WRF-Chem, and (c, f) XCO_2 by WRF-CO₂ over East Asia at (left) 0100 and (right) 0600 local time (LT) on December 9, 2016.

5e, and 5f). Simulated $\text{PM}_{2.5}$ are evaluated using surface air quality station data and hourly statistic metrics are calculated (Table 2). The performance of simulated $\text{PM}_{2.5}$ are comparable to previous WRF-Chem air quality simulations (e.g., Hu, 2008), e.g., in terms of correlation coefficient (r), and normalized mean bias (NMB). The model shows higher r and lower NMB on 9 December 2016 (Table 2 and Figure S2 in Supporting Information) when the horizontal gradient of pollutants is prominent when the cold front is present in the domain, which indicates that model captures the spatial variability better when such variability is significant and has large scale characteristics.

Note that the meteorological fields from the WRF-Chem and WRF-CO₂ simulations are similar in terms of synoptic meteorology and boundary layer structures (Figure 7), which are most relevant to transport/dispersion of atmospheric constituents discussed in this study. Thus, only meteorological fields from the WRF-Chem simulation are shown (Figures 5, 6 and 8). Ahead of the front, strong stability near the surface (as indicated by the potential temperature inversion in Figure 7) leads to low boundary layer height, e.g., at Nanchang and Quzhou (Figures 7c and 7d). Behind the front, stronger wind induces stronger mechanical turbulence, reducing the stability and enhancing boundary layer height, e.g., at Sheyang and Shanghai (Figures 6 and 7a, 7b). More discussion regarding boundary layer structure/heights, and thermal stability over China during winter can be found in Miao and Liu (2019). The surface temperature contrast across the front (Figure 6a) is not as crisp and clear as the contrast of equivalent potential temperature (θ_e) in the boundary layer (Figures 5a and 5d) likely because the large disturbance of heterogeneity of land surface, as

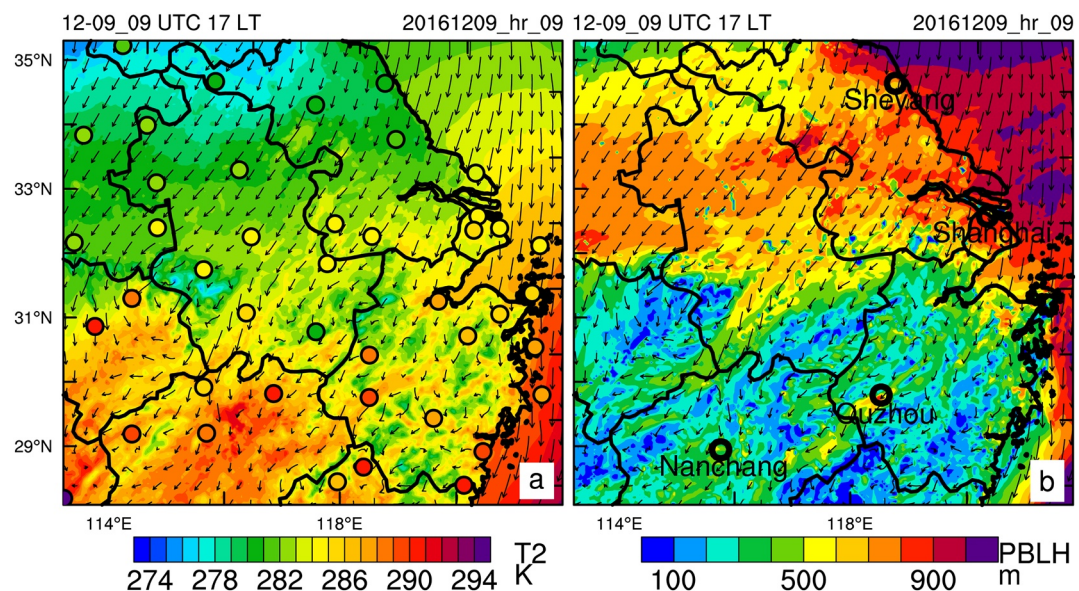


Figure 6. Spatial distribution of (a) simulated 2-m temperature (T2) and 10-m wind vectors with the National Climatic Data Center (NCDC) Global Hourly Surface Data overlaid using shaded circles, and (b) simulated PBL height by WRF-Chem at 1700 local time on December 9, 2016.

well as terrain height difference in the region (Figure 1). The contrast of boundary layer height across the front (Figure 6b) is also more prominent than that of surface temperature (Figure 6a) because boundary layer height has a larger footprint (i.e., affected by more upstream air mass) and is less affected by local surface heterogeneity.

The cold front sweeps and cleans up the North China Plains and all the emitted species (and some secondary pollutants) are accumulated at the leading edge, including PM_{2.5} and XCO₂ (Figure 5). Bands of elevated pollutant concentrations along frontal edges have also been reported previously (Hu et al., 2019). Since CO₂ and some primary pollutants (e.g., NO_x = NO + NO₂, SO₂, CO, and soot particles) are often coemitted (Konovalov et al., 2016; Lopez et al., 2013; Silva & Arellano, 2017; Tang et al., 2019), their spatial distributions (e.g., between CO₂ and NO) are similar (Figure 3). The correlation between emissions of CO₂ and NO varies between 0.77 and 0.86 at grid spacings of 40–100 km. Note that even though both NO and NO₂ are produced from combustion process, most air quality emission inventories, including the one used in this study, assign most NO_x emission into NO. NO_x, SO₂, and soot particles are all important precursors/components of PM_{2.5} in the region (Li, Wang, et al., 2019). As a result of similar emission distribution, the band region with elevated concentrations of PM_{2.5} and XCO₂ ahead of the front resemble each other (Figure 5). Thus, adding an WRF-CO₂ simulation to a conventional WRF-Chem air quality simulation could provide additional/corroborating information regarding air pollution events (particularly in terms of spatial distribution), serving similar purposes as the multimodel approach used in other air quality studies, which include deriving the most robust information in presence of all sorts of model errors (Fiore et al., 2009; Leibensperger et al., 2011).

The different physics configurations between WRF-Chem and WRF-CO₂ simulation are radiation schemes. While WRF-Chem simulation used RRTMG shortwave and longwave radiation schemes (Iacono et al., 2008), WRF-CO₂ simulation used Dudhia shortwave radiation scheme (Dudhia, 1989), and the rapid radiative transfer model (RRTM) (Mlawer et al., 1997) for longwave radiation. We repeat the WRF-CO₂ simulation with RRTMG shortwave and longwave radiation schemes to be consistent with the WRF-Chem simulation. Despite the slight sensitivity to radiation schemes (Figure S3 in Supporting Information), the WRF-CO₂ simulations with both radiation configurations, are able to capture the sharp rise of CO₂ associated with the cold front passage (Figure S4 in Supporting Information), coincident with the sharp rise of PM_{2.5} (Figure 4). Thus, this additional simulation further corroborates our conclusion: WRF-CO₂ simulation, despite with its own uncertainties associated with physics parameterizations, can be used to help

Table 2
Hourly Statistics^a Evaluation for the Simulated PM_{2.5} on December 9, 2016 at 389 Air Quality Sites in Eastern China in the Second Domain

Time, hour	12/9	1	2	3	4	5	6	7	8	9	10	11	12	13	14	15	16	17	18	19	20	21	22	23	12/10
Mean Obs, μg m ⁻³	136.6	132	127.4	127.9	128.2	125.4	118.8	112.9	109.3	107.0	103.2	99.8	93.7	91.9	86.1	81.4	78.3	76.9	78.9	81.8	81.9	78.7	75.1	70.6	68.6
Mean Sim, μg m ⁻³	153.7	143.8	136.5	130.3	123.4	115.9	113.3	117.0	121.5	113.9	116.5	111.0	106.5	102.5	98.4	96.7	96.9	100.5	107.7	107.4	103.1	102.1	100.7	93.4	88.7
Number	384	388	389	388	386	386	386	386	386	386	386	383	386	385	386	384	386	385	384	385	385	385	386	385	
<i>r</i>	0.16	0.23	0.29	0.27	0.28	0.29	0.28	0.21	0.21	0.26	0.36	0.45	0.53	0.50	0.51	0.43	0.45	0.43	0.38	0.37	0.47	0.54	0.51	0.48	0.49
MB, μg m ⁻³	17.1	11.8	9.1	2.4	-4.8	-9.5	-5.5	4.1	12.3	7.0	13.3	11.3	12.8	10.6	12.3	15.3	18.7	23.6	28.9	25.7	21.2	23.5	25.6	22.8	20.2
MAGE, μg m ⁻³	61.7	55.2	52.1	50.4	50.3	49.0	46.2	48.8	50.2	42.9	44.9	43.0	39.5	38.6	38.5	39.4	39.3	41.8	47.4	47.8	42.9	40.7	41.9	40.1	38.9
RMSE, μg m ⁻³	87.1	76.5	71.5	67.4	64.7	63.4	61.3	65.6	67.5	57.9	60.9	60.3	57.4	59.8	57.1	60.0	59.8	60.7	65.2	63.5	54.4	50.1	51.2	49.2	46.8
NMB, %	12.5	8.9	7.1	1.9	-3.7	-7.6	-4.6	3.6	11.2	6.5	12.9	11.3	13.6	11.5	14.3	18.7	23.8	30.7	36.6	31.4	25.9	29.8	34.1	32.3	29.4

^aThe statistical metrics include: correlation coefficient (*r*), mean bias (MB), mean absolute gross error (MAGE), root mean-square error (RMSE), and normalized mean bias (NMB). Formulas for these metrics can be found in Seigneur et al. (2000). These statistical metrics are commonly used in numerical air quality model evaluations (e.g., Han et al., 2008; Hu et al., 2013, 2020; Yu et al., 2006; Zhang, Chen, et al., 2014).

forecast and investigate air pollution events, collectively with other air quality simulations and observations.

After reaching the Yangtze River Delta Region, the leading edge of the cold front was partially blocked by terrain, and hence separated when further penetrating southward (Figure 8). At 0400 local time on December 9, 2016, the NO and XCO₂ bands are still relatively smooth and undisturbed over a flat terrain region (Figures 8b and 8c). Later on, the southward-penetrating front is blocked by the Mountains Huang and Dabie. At 1600 local time, a channel flow (also referred to as gap winds at times, e.g., Overland & Walter, 1981) between Mountain Huang and Mountain Dabie is prominent, while the rest of the front appears stalled (Figure 8d). The channel winds accelerate along the channel and reach maximum near the southern end of the channel following the Bernoulli principle, i.e., total pressure (sum of static pressure and dynamic pressure (expressed as a function of square of wind speeds)) is conserved in a surface streamline (Hitzl et al., 2020; Zhang et al., 2005):

$$u^2 = u_0^2 - 2 \cdot \frac{\Delta p}{\rho}, \quad (1)$$

where u_0 and u are the initial and exit wind speed along the gap, Δp is the pressure change, ρ is air density. High static pressure resides over the North China Plains and the Yangtze River Delta Region on this day (Figure 2). Thus, the static pressure is higher when the flow enters the channel and decreases along the channel (Figure S2). Consequently, wind speeds increase along the channel according to the Bernoulli conservation. As a quantitative example, at 1800 local time, the initial wind is $\sim 8 \text{ m s}^{-1}$, and pressure changes by 2 hPa along the gap. According to Equation 1, the wind at the exit of the gap is about to increase by 12 m s^{-1} . However, surface drag and vertical entrainment can reduce the acceleration by almost 50% (Zhang et al., 2005). The simulated wind speed at the exit of the gap $\sim 13\text{--}14 \text{ m s}^{-1}$ matches well with the Bernoulli theory (Figure S5 in Supporting Information).

The channel flow brings plume of pollutants (e.g., NO, Figure 8e, AOD, Figure 9a) from the North China Plains and Yangtze River Delta Region into Jiangxi province, contributing to the air pollution in the region. This regional transport is confirmed by the WRF-CO₂ simulation (Figure 8f), as well as a few satellite sensors (Figure 9). Three satellite retrieval products, MODIS AOD, OMPS NO₂, and AIRS CO, all illustrate a stalled band of elevated pollutant concentrations along the Yangtze River Delta Region and this pollution plume only leaks into the Jiangxi province through the narrow Dabie-Huang channel as indicated by the AOD data with a resolution of $3 \times 3 \text{ km}^2$. Interestingly, the penetration/leaking is visible in the elevated AOD and XCO₂ concentration bands, despite being column integrated quantities. OMPS NO₂ and AIRS CO have lower resolutions ($\sim 50 \times 50 \text{ km}^2$), thus do not resolve the channel transport as well as the MODIS AOD data, with AIRS CO still showing a discernable plume extending into Jiangxi through the Dabie-Huang channel (Figure 9d). MOPITT aboard the Terra satellite observes CO with a higher resolution ($22 \times 22 \text{ km}^2$), but at a different overpassing time from the other satellite data used in this study, thus is not used here. Note that we use AIRS CO at $\sim 500 \text{ mb}$ where the retrieval is the most sensitive. Frontal structure (as well as constituents) at $\sim 500 \text{ mb}$ may not exactly align with the surface front (Hu et al., 2020), which further explains why the detected elevated CO concentration band is relatively diffuse.

Such a regional transport pathway is further illustrated using simulated and observed surface PM_{2.5} as well as simulated CO (Figure 10). PM_{2.5} concentration at Jiujiang peaks at 1800 local time, about 2 h later after PM_{2.5} peaking at Anqing, a site north to Jiujiang between the Dabie-Huang channel, corroborating the southward

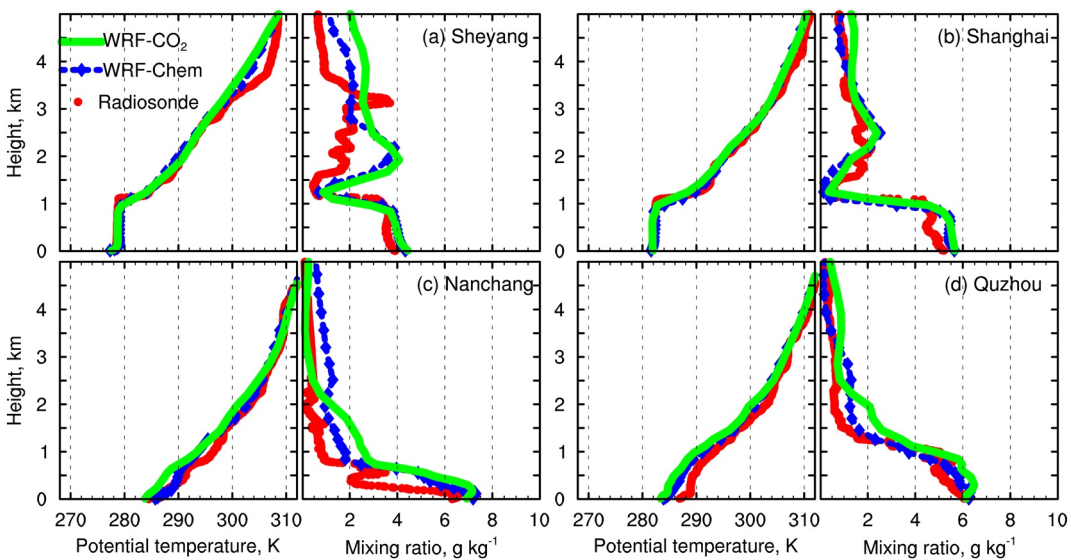


Figure 7. Observed and simulated profiles at (a, b) Sheyang and Shanghai (behind of the front) and (c, d) Nanchang and Quzhou (ahead of the front) at 1900 local time on December 9, 2016.

transport of the haze plume through the Dabie-Huang channel. At 2000 local time, the pollution plume (as indicated by both CO and PM_{2.5}) farther penetrates southward and reaches Nanchang, contributing to the haze pollution in the region (Figure 10). Thus, while previous studies pointed out the importance of local sources on air quality in Jiangxi province, including vehicles, industries, waste burning, and dust (Yang et al., 2017; Zhao et al., 2017), this study illustrates that air pollution in Jiangxi province may be affected by pollutants transported from the North China Plain and Yangtze River Delta Region through the Dabie-Huang channel. In such scenarios, monitoring the air pollution at sites along the Dabie-Huang channel (e.g., Anqing and Jiujiang) may be indicative and informative for the air quality prediction in the rest of the Jiangxi province.

Corroborating evidence from observed and simulated pollutants, simulated XCO₂ also reveals the regional transport characteristics. The spatial distributions of simulated XCO₂ and MODIS AOD are consistent (Figures 9a and 9b) with a correlation of 0.8 (Figure 11). Note that some of the AOD over the western domain is not available due to the presence of cloud (figure not shown) or poor retrieval quality. The high correlation between simulated XCO₂ and MODIS AOD is comparable to previously reported correlation between simulated and observed AOD (Basart et al., 2012; Hu, 2008; Matthias, 2008; Pere et al., 2010; Roy et al., 2007). The comparable correlations imply that the uncertainties in air quality simulations when simulating aerosol and AOD may be comparable to the spread of simulated concentrations of different but coemitted species. This also illustrates that WRF-CO₂ simulations can help constrain air pollution prediction uncertainties, at least for AOD to a quite high extent for this studied case.

To more quantitatively estimate the contribution of regional transport to the pollution in the middle and lower reaches of the Yangtze River region, WRF-CO₂ tracer simulations are conducted with turning on/off anthropogenic CO₂ emissions over the North China Plain (NCP) for the December 6–9 episode. The emissions over the NCP contributes ~20 ppm CO₂ at the leading edge of the front (Figure 12b), accounting for up to 70% of total anthropogenic CO₂, particularly in rural areas in the middle and lower reaches of the Yangtze River region (Figure 12c). Over the ocean east of the Yangtze Delta region, the contribution from NCP emissions exceeds 95% because the CO₂ plume over the ocean was swept off the NCP on December 8 and transported southward on December 9. Over the large emission sources (e.g., Shanghai, Suzhou, Nanjing, and Huainan) and the downwind regions, the contribution of regional transport of NCP emissions decreases to <50%. The contribution of regional transport of NCP emissions to the area south of Hangzhou becomes insignificant (<10%). For PM_{2.5}, the contribution of regional transport is more complex since secondary aerosols are involved, thus needs more careful examination (Li, Wang, et al., 2019; Sun et al., 2020).

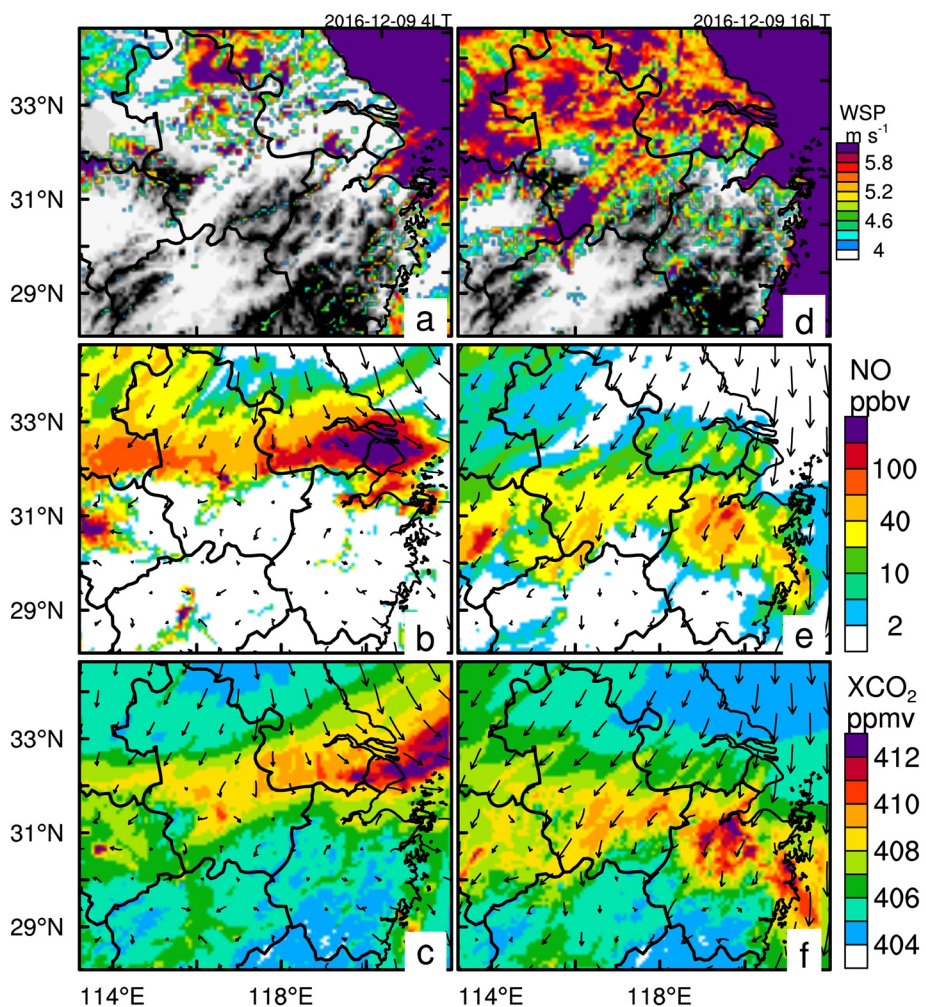


Figure 8. Spatial distribution of simulated (a, d) surface wind speed, and (b, e) NO by WRF-Chem, and (c, f) XCO₂ by WRF-CO₂ at (left) 0400 and (right) 1600 local time on December 9, 2016.

The synoptic condition of December 9, 2016 falls into the Type 1 synoptic pattern classified by Xiao et al. (2020), which is characterized by northerly prevailing winds transporting polluted air from the North China Plains to the middle and lower reaches of the Yangtze River region from Wuhan to Shanghai. Such a synoptic pattern accounts for 31.8% of time in a year (Xiao et al., 2020).

On December 9, OCO-2 passed through the Shanghai-Hangzhou metropolitan area. The XCO₂ data at 1:30 PM local time capture the plume in the Hangzhou metropolitan area, showing a good agreement with the WRF-CO₂ simulation and thus providing confidence in the simulated XCO₂ (Figure 9b). Given the high correlation, satellite XCO₂ data can thus provide an extra and corroborating technique to monitor air pollution, in addition to existing surface networks and other remote-sensing instruments.

In addition to the case of December 9, 2016, Figure 13 shows four other CO₂ plumes in the Yangtze River Delta Region captured by OCO-2 XCO₂ data, with different plume characteristics, on April 29, 2016, March 15, 2017, February 5, and March 9, 2018. During the first two cases, OCO-2 XCO₂ captures the plumes around the Shanghai metropolitan area, with the plumes blown into different directions. During the last two cases, OCO-2 XCO₂ captures the plumes emanated from Nanjing and Yangzhou, also with different prevailing winds (westerly on February 5 and northerly on March 9, 2018) as indicated by the plume directions. These cases corroborate that even though XCO₂ variation caused by anthropogenic activities (about a few ppmv) is very small comparing to the large background value (on the order of 400 ppmv) (Shim et al., 2019),

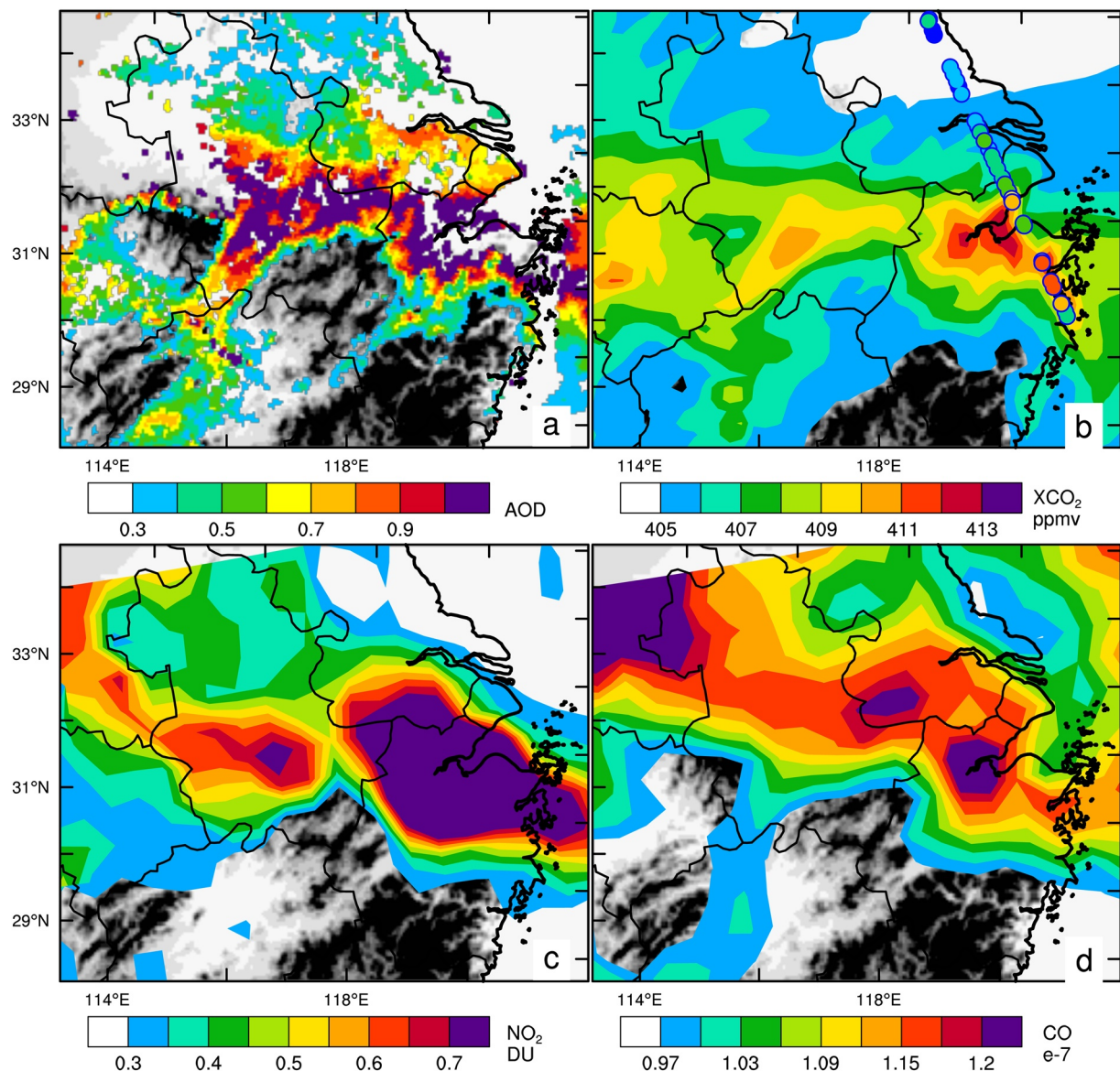


Figure 9. (a) MODIS AOD, (b) simulated XCO₂ overlaid with OCO-2 observation, (c) OMPS NO₂, and (d) AIRS CO on December 9, 2016.

high-precision OCO-2 XCO₂ data are able to capture these regional to urban scale anthropogenic CO₂ plumes (Eldering et al., 2017; O'Dell et al., 2018). Thus, OCO-2 XCO₂ can be used as a proxy variable to monitor other coemitted species, as well as secondary pollutants such as PM_{2.5}; together with other observations and simulations, OCO-2 XCO₂ can collectively provide useful information to monitor and predict haze pollutions that plague China and other regions over the world.

4. Discussion on Using XCO₂ Data to Capture Urban CO₂ Plumes

As shown above, the OCO-2 XCO₂ data can be used to collectively monitor and predict air pollution with other instruments and models, particularly when the gradient of air pollution is large in the meridional direction. OCO-2 collects soundings at 0.333-s intervals across a narrow swath with a footprint of 2.25 × 1.29 km², thus proving a high frequency coverage along the meridional direction. However, its long repeat cycle (16 days) in terms of longitude coverage and a few other factors limit wide application of OCO-2

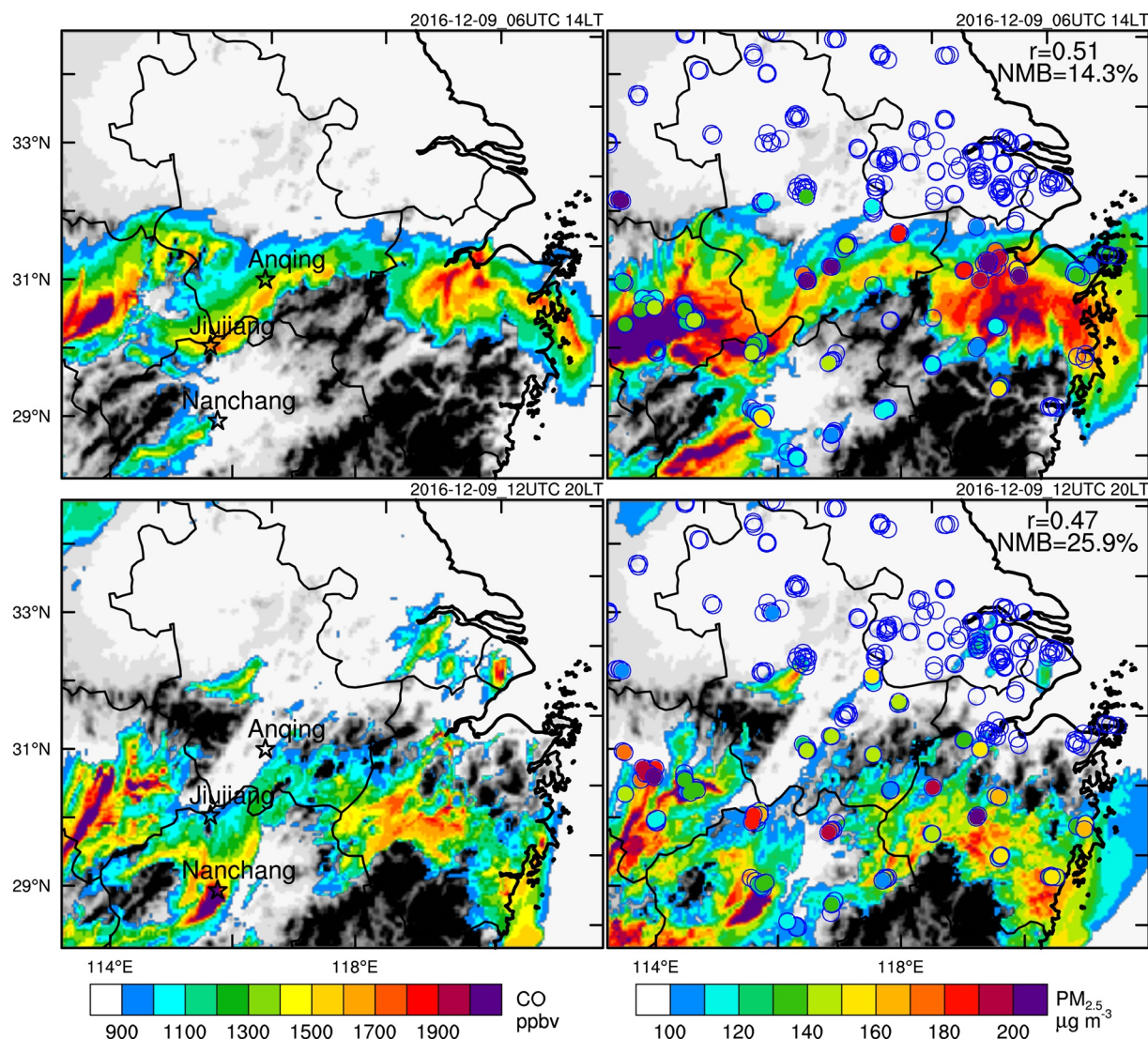


Figure 10. Spatial distribution of (left) CO and (right) PM_{2.5} simulated by WRF-Chem overlaid with surface observation of PM_{2.5} at (top) 1400 and (bottom) 2000 local time, on December 9, 2016. Open circles mean PM_{2.5} values <100 µg m⁻³. Hourly statistic metrics of PM_{2.5} evaluated using surface observations are marked, including correlation coefficient (r), and normalized mean bias (NMB).

XCO₂ data. On any given day, adjacent OCO-2 tracks are separated by $\sim 25^\circ$ of longitude. After each 16-days cycle, the gaps between OCO-2 tracks are ~ 1.6 ($25/16$)° (Crisp et al., 2017; Kulawik, Crowell, et al., 2019). In addition, OCO-2 retrieval of XCO₂ becomes unreliable and not usable in presence of clouds, as with many other satellite products (O'Dell et al., 2018). Thus OCO-2 XCO₂ coverage in longitude direction is sparse and may not pass over certain urban areas on a given day, which limits its wide application for detecting urban scale pollutions. Instead, regional scale pollution covering a wider range of longitude may be more likely captured by the OCO-2 XCO₂ data. However, in the upcoming years, emerging wider coverage of XCO₂ satellite data (e.g., from OCO-3) will provide more frequent urban pollution information (Wu et al., 2020).

Also, OCO-2 XCO₂ retrieval can be interfered by presence of aerosol (O'Dell et al., 2018), which may cause an interfere error of 0.2–1.0 ppmv (Chen, Liu, Yang, et al., 2019). The regional enhancement of XCO₂ in the Yangtze River Delta Region is ~ 7 ppmv for the December 9 episode examined in this study (Figure 9b). Other studies (e.g., Shim et al., 2019) estimate the regional enhancement of XCO₂ in the metropolitan areas such as South Korea to be around 7.3–10.7 ppmv. Thus, at least in these regions, the regional to urban enhancement of XCO₂ is much larger than the interference error associated with aerosols, thus won't be

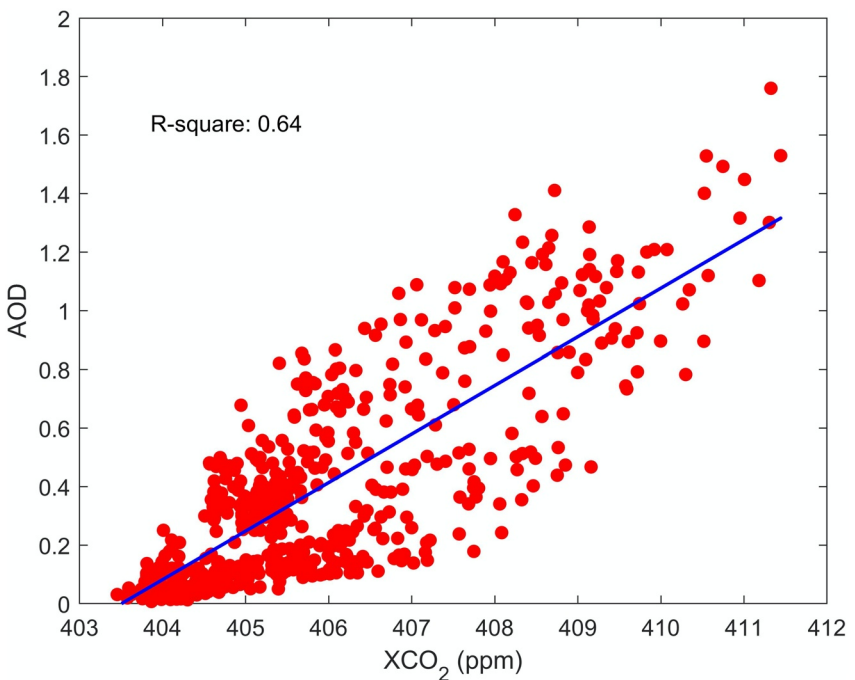


Figure 11. Correlation between MODIS AOD and simulated XCO_2 at 1:30 PM on December 9, 2016.

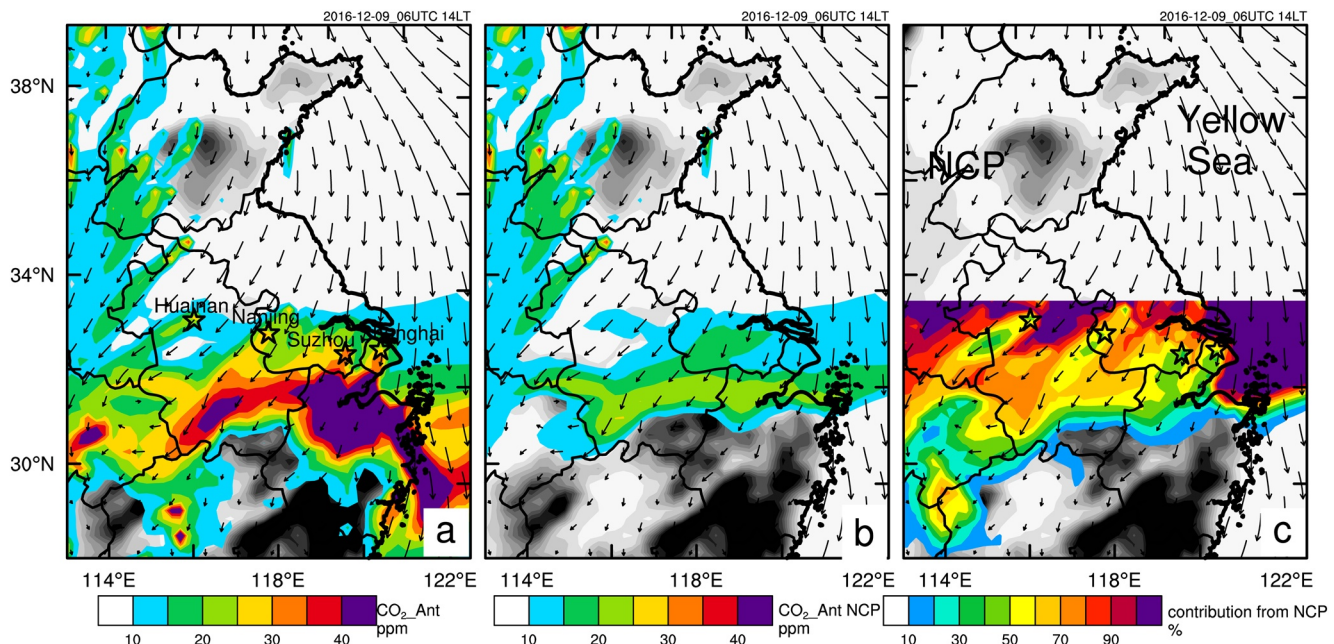


Figure 12. Spatial distribution of (a) total anthropogenic CO_2 and (b) contribution from emissions from the North China Plain (NCP), and (c) contribution percentage over the middle and lower reaches of the Yangtze River region at 1400 local time on December 9, 2016. Four cities with large anthropogenic CO_2 emissions in the Yangtze River region (from east to west), Shanghai, Suzhou, Nanjing, and Huainan, are marked with stars.

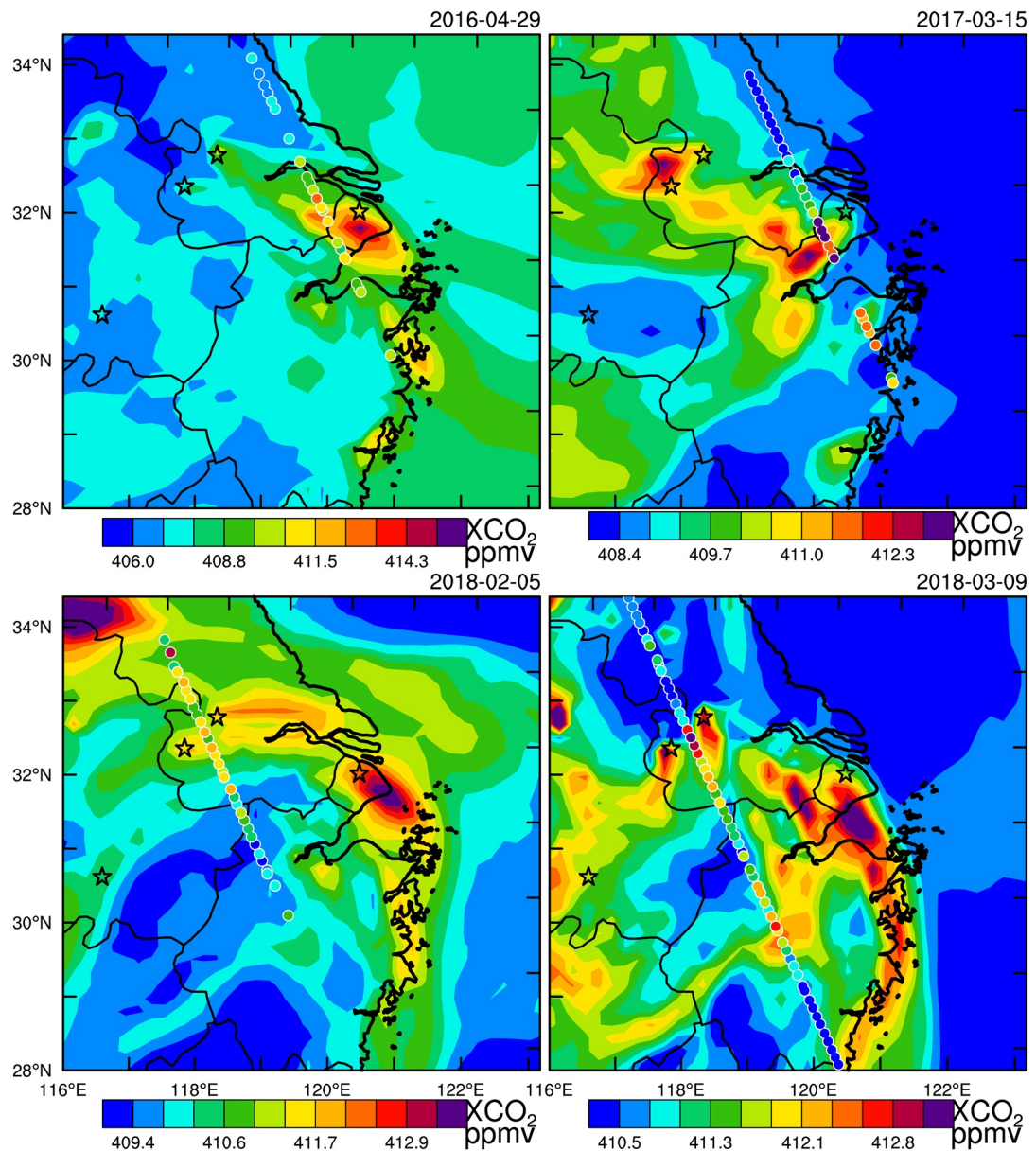


Figure 13. Simulated XCO₂ overlaid with OCO-2 data for four additional cases with OCO-2 passing over the urban plumes in the Yangtze River Delta Region. Anqing, Nanjing, Yangzhou, and Shanghai (from left to right) are marked with stars.

masked by the interference error. Nevertheless, an optimized XCO₂ retrieval algorithm to reduce XCO₂ uncertainties associated with aerosols is warranted (Chen, Liu, Yang, et al., 2019; Kulawik, O'Dell, et al., 2019).

5. Conclusions and Discussion

A severe haze pollution event on December 9, 2016 in the Yangtze River Delta Region is investigated using multisensors (including satellites MODIS, OCO-2, AIRS, OMPS, as well as surface instruments) and multimodels, including WRF-Chem and WRF-CO₂. On this day, a cold front penetrated southward from the North China Plain to the Yangtze River Delta Region. While this front cleaned the North China Plain, pollutants accumulated at its leading edge (as well as the greenhouse gas CO₂), which exacerbated air pollution over the Yangtze River Delta Region. While most previous studies emphasized that frontal systems

associated with midlatitude baroclinic cyclones replace polluted continental air with cleaner air, thus improving air quality (Leibensperger et al., 2008; Liu et al., 2017), this study calls attention for pollution around the leading edge of fronts. Such a pollution mechanism also provides a plausible explanation for the heavy pollutions observed in central China at times, where emissions are relatively less heavy (Xiao et al., 2020; Yu et al., 2020). A similar mechanism for air pollution formation was previously reported by Hu et al. (2019) over the South Great Plains.

Later on December 9, the front became distorted due to terrain blocking. The channel winds between Mountains Dabie and Huang pushed the front forward and transported the haze plume into Jiangxi province, enhancing the pollution in the region. This pollution event in terms of its spatial coverage and regional transport characteristics was corroborated by observations from multiple satellite sensors, including MODIS AOD, OCO-2 XCO₂, OMPS NO₂, and AIRS CO, as well as surface air quality sites.

This air pollution event is well reproduced by the WRF-Chem simulation, particularly in terms of its spatial coverage. CO₂ simulated by WRF-CO₂ also indicates a similar spatial distribution, because CO₂ is often coemitted with other pollutants (or precursors) and thus their distributions have high correlations. Given the limitations in the spatial coverage of surface air quality sites and instrumental errors, as well as uncertainties of emissions and air quality models, monitoring and prediction of air pollution events in China are less confident than in data-richer regions such as the United States. This study demonstrates that using more sensors, particularly satellite sensors (including XCO₂ spectrometer) together with WRF-CO₂ simulations, in addition to conventional in-situ measurements and air quality simulations, can collectively better monitor bulk anthropogenic activity, examine and predict air pollution events, particularly in terms of their spatial distribution and regional transport. To the best of our knowledge, this study is the first one to demonstrate that satellite XCO₂ data and WRF-CO₂ simulation can be used to help monitor and predict air quality (e.g., in terms of urban plumes and transboundary pollution), given that CO₂ emissions have a similar distribution as emissions of pollutants.

In this study, CO₂ and air pollutants are simulated separately using WRF-CO₂ and WRF-Chem, respectively. If the VPRM model and other modifications in WRF-CO₂ are also implemented into WRF-Chem, the resulting system can then be used to simulate CO₂ together with other chemical species pertaining to air quality. Simulating CO₂ and air pollutants simultaneously in one modeling system is appealing and warranted given that CO₂ and some pollutants are coemitted, and they have similar spatiotemporal variations as demonstrated in this study. Such an implementation can be pursued in the future.

For the first time, we illustrate that pollutants may be transported from the North China Plain and Yangtze River Delta Region to Jiangxi province through the Dabie-Huang channel, contributing to the air pollution in the region. Thus, monitoring chemical and meteorological variables along the Dabie-Huang channel is important for predicting air quality in Jiangxi province. More quantitative estimation of contribution from such regional transport is warranted for air quality assessment and design of emission abatement strategy in Jiangxi. Such a quantitative estimation needs to be conducted with air quality simulations with accurate calculation of secondary inorganic aerosols, particularly sulfate, nitrate, and ammonium, due to their significant contribution (Li, Wang, et al., 2019; Sun et al., 2020).

Data Availability Statement

The reanalysis data set was downloaded from <https://rda.ucar.edu/>, the CT2017 data were provided by NOAA ESRL, Boulder, Colorado, USA from the website at <http://carbontracker.noaa.gov>. MODIS AOD is downloaded from <https://ladsweb.modaps.eosdis.nasa.gov/> and other satellite data are downloaded from <https://disc.gsfc.nasa.gov/>. The NCDC data used for model evaluation are downloaded from <http://www7.ncdc.noaa.gov/CDO/cdo>, and the radiosonde data are archived by the China Metrological Administration (CMA). Danhua Zhai provided the weather map in Figure 2. Model data produced from this study have been archived at the Luster NSF projects data server at the San Diego Supercomputer Center, /expanse/luster/projects/uok114/xhu2.

Acknowledgments

The first author was partially supported by NSF Grant AGS-1917701. Computations were performed at the San Diego Supercomputer Center (SDSC) through XSEDE allocation grant TG-ATM160014.

References

- Ackermann, I. J., Hass, H., Memmesheimer, M., Ebel, A., Binkowski, F. S., & Shankar, U. (1998). Modal aerosol dynamics model for Europe: Development and first applications. *Atmospheric Environment*, 32(17), 2981–2999. [https://doi.org/10.1016/S1352-2310\(98\)00006-5](https://doi.org/10.1016/S1352-2310(98)00006-5)
- Ahmadov, R., Gerbig, C., Kretschmer, R., Koerner, S., Neininger, B., Dolman, A. J., & Sarrat, C. (2007). Mesoscale covariance of transport and CO₂ fluxes: Evidence from observations and simulations using the WRF-VPRM coupled atmosphere-biosphere model. *Journal of Geophysical Research*, 112, D22107. <https://doi.org/10.1029/2007JD008552>
- Andres, R. J., Boden, T. A., & Higdon, D. (2014). A new evaluation of the uncertainty associated with CDIAC estimates of fossil fuel carbon dioxide emission. *Tellus B: Chemical and Physical Meteorology*, 66(1), 23616. <https://doi.org/10.3402/tellusb.v66.23616>
- Basart, S., Pay, M. T., Jorba, O., Perez, C., Jimenez-Guerrero, P., Schulz, M., & Baldasano, J. M. (2012). Aerosols in the CALIOPE air quality modelling system: Evaluation and analysis of PM levels, optical depths and chemical composition over Europe. *Atmospheric Chemistry and Physics*, 12(7), 3363–3392. <https://doi.org/10.5194/acp-12-3363-2012>
- Binkowski, F. S., & Roselle, S. J. (2003). Models-3 Community Multiscale Air Quality (CMAQ) model aerosol component 1. Model description. *Journal of Geophysical Research*, 108(D6), 4183. <https://doi.org/10.1029/2001JD001409>
- Bouarar, I., Brasseur, G., Petersen, K., Granier, C., Fan, Q., Wang, X. M., et al. (2019). Influence of anthropogenic emission inventories on simulations of air quality in China during winter and summer 2010. *Atmospheric Environment*, 198, 236–256. <https://doi.org/10.1016/j.atmosenv.2018.10.043>
- Brioude, J., Angevine, W. M., Ahmadov, R., Kim, S. W., Evan, S., McKeen, S. A., et al. (2013). Top-down estimate of surface flux in the Los Angeles Basin using a mesoscale inverse modeling technique: Assessing anthropogenic emissions of CO, NOx and CO₂ and their impacts. *Atmospheric Chemistry and Physics*, 13(7), 3661–3677. <https://doi.org/10.5194/acp-13-3661-2013>
- Brioude, J., Petron, G., Frost, G. J., Ahmadov, R., Angevine, W. M., Hsie, E. Y., et al. (2012). A new inversion method to calculate emission inventories without a prior at mesoscale: Application to the anthropogenic CO₂ emission from Houston, Texas. *Journal of Geophysical Research*, 117, D05312. <https://doi.org/10.1029/2011JD016918>
- Byun, D., & Schere, K. L. (2006). Review of the governing equations, computational algorithms, and other components of the Models-3 Community Multiscale Air Quality (CMAQ) modeling system. *Applied Mechanics Reviews*, 59(2), 51–77. <https://doi.org/10.1115/1.2128636>
- Chen, D., Liu, Z. Q., Ban, J. M., & Chen, M. (2019). The 2015 and 2016 wintertime air pollution in China: SO₂ emission changes derived from a WRF-Chem/EnKF coupled data assimilation system. *Atmospheric Chemistry and Physics*, 19(13), 8619–8650. <https://doi.org/10.5194/acp-19-8619-2019>
- Chen, F., & Dudhia, J. (2001). Coupling an advanced land surface-hydrology model with the Penn State-NCAR MM5 modeling system. Part I: Model implementation and sensitivity. *Monthly Weather Review*, 129(4), 569–585. [https://doi.org/10.1175/1520-0493\(2001\)129<0569:Caalsh>2.0.Co;2](https://doi.org/10.1175/1520-0493(2001)129<0569:Caalsh>2.0.Co;2)
- Chen, L., Zhu, J., Liao, H., Gao, Y., Qiu, Y., Zhang, M., et al. (2019). Assessing the formation and evolution mechanisms of severe haze pollution in the Beijing-Tianjin-Hebei region using process analysis. *Atmospheric Chemistry and Physics*, 19(16), 10845–10864. <https://doi.org/10.5194/acp-19-10845-2019>
- Chen, X., Liu, Y., Yang, D. X., Cai, Z. N., Chen, H. B., & Wang, M. H. (2019). A theoretical analysis for improving aerosol-induced CO₂ retrieval uncertainties over land based on TanSat Nadir observations under clear sky conditions. *Remote Sensing*, 11(9), 1061. <https://doi.org/10.3390/RS11091061>
- Ciais, P., Sabine, C., Bala, G., Bopp, L., Brovkin, V., Canadell, J., et al. (2014). Carbon and other biogeochemical cycles. In C. Intergovernmental Panel on Climate (Ed.), *Climate change 2013—The physical science basis: Working group I contribution to the fifth assessment report of the intergovernmental panel on climate change* (pp. 465–570). Cambridge: Cambridge University Press.
- Colette, A., Andersson, C., Manders, A., Mar, K., Mircea, M., Pay, M. T., et al. (2017). EURODELTA-Trends, a multi-model experiment of air quality hindcast in Europe over 1990–2010. *Geoscientific Model Development*, 10(9), 3255–3276. <https://doi.org/10.5194/gmd-10-3255-2017>
- Colette, A., Granier, C., Hodnebrog, O., Jakobs, H., Maurizi, A., Nyiri, A., et al. (2011). Air quality trends in Europe over the past decade: A first multi-model assessment. *Atmospheric Chemistry and Physics*, 11(22), 11657–11678. <https://doi.org/10.5194/acp-11-11657-2011>
- Colette, A., Granier, C., Hodnebrog, O., Jakobs, H., Maurizi, A., Nyiri, A., & Vrac, M. (2012). Future air quality in Europe: A multi-model assessment of projected exposure to ozone. *Atmospheric Chemistry and Physics*, 12(21), 10613–10630. <https://doi.org/10.5194/acp-12-10613-2012>
- Crisp, D., Atlas, R. M., Breon, F. M., Brown, L. R., Burrows, J. P., Ciais, P., et al. (2004). The orbiting carbon observatory (OCO) mission. *Trace Constituents in the Troposphere and Lower Stratosphere*, 34(4), 700–709. <https://doi.org/10.1016/j.jasr.2003.08.062>
- Crisp, D., Miller, C. E., & DeCola, P. L. (2008). NASA Orbiting Carbon Observatory: Measuring the column averaged carbon dioxide mole fraction from space. *Journal of Applied Remote Sensing*, 2, 023508. <https://doi.org/10.1117/1.2898457>
- Crisp, D., Pollack, H. R., Rosenberg, R., Chapsky, L., Lee, R. A. M., Oyafuso, F. A., et al. (2017). The on-orbit performance of the Orbiting Carbon Observatory-2 (OCO-2) instrument and its radiometrically calibrated products. *Atmospheric Measurement Techniques*, 10(1), 59–81. <https://doi.org/10.5194/amt-10-59-2017>
- Ding, A. J., Fu, C. B., Yang, X. Q., Sun, J. N., Zheng, L. F., Xie, Y. N., et al. (2013). Ozone and fine particle in the western Yangtze River Delta: An overview of 1 yr data at the SORPES station. *Atmospheric Chemistry and Physics*, 13(11), 5813–5830. <https://doi.org/10.5194/acp-13-5813-2013>
- Dong, X. Y., Fu, J. S., Zhu, Q. Z., Sun, J., Tan, J. N., Keating, T., et al. (2018). Long-range transport impacts on surface aerosol concentrations and the contributions to haze events in China: An HTAP2 multi-model study. *Atmospheric Chemistry and Physics*, 18(21), 15581–15600. <https://doi.org/10.5194/acp-18-15581-2018>
- Donkelaar, A. V., Martin, R. V., Brauer, M., Kahn, R., Levy, R., Verduzco, C., & Villeneuve, P. J. (2010). Global estimates of ambient fine particulate matter concentrations from satellite-based aerosol optical depth: Development and application. *Environmental Health Perspectives*, 118(6), 847–855. <https://doi.org/10.1289/ehp.0901623>
- Dudhia, J. (1989). Numerical study of convection observed during the winter monsoon experiment using a mesoscale two-dimensional model. *Journal of the Atmospheric Sciences*, 46(20), 3077–3107. [https://doi.org/10.1175/1520-0469\(1989\)046<3077:Nsocod>2.0.Co;2](https://doi.org/10.1175/1520-0469(1989)046<3077:Nsocod>2.0.Co;2)
- Eldering, A., O'Dell, C. W., Wennberg, P. O., Crisp, D., Gunson, M. R., Viatte, C., et al. (2017). The Orbiting Carbon Observatory-2: First 18 months of science data products. *Atmospheric Measurement Techniques*, 10(2), 549–563. <https://doi.org/10.5194/amt-10-549-2017>
- Emmons, L. K., Walters, S., Hess, P. G., Lamarque, J. F., Pfister, G. G., Fillmore, D., et al. (2010). Description and evaluation of the model for ozone and related chemical tracers, version 4 (MOZART-4). *Geoscientific Model Development*, 3(1), 43–67.

- Fast, J. D., Gustafson, W. I. Jr., Easter, R. C., Zaveri, R. A., Barnard, J. C., Chapman, E. G., et al. (2006). Evolution of ozone, particulates, and aerosol direct radiative forcing in the vicinity of Houston using a fully coupled meteorology-chemistry-aerosol model. *Journal of Geophysical Research*, 111, D21305. <https://doi.org/10.1029/2005JD006721>
- Fiore, A. M., Dentener, F. J., Wild, O., Cuvelier, C., Schultz, M. G., Hess, P., et al. (2009). Multimodel estimates of intercontinental source-receptor relationships for ozone pollution. *Journal of Geophysical Research*, 114, D04301. <https://doi.org/10.1029/2008JD010816>
- Fu, Z. Y., & Li, R. (2020). The contributions of socioeconomic indicators to global PM_{2.5} based on the hybrid method of spatial econometric model and geographical and temporal weighted regression. *Science of the Total Environment*, 703, 135481. <https://doi.org/10.1016/j.scitotenv.2019.135481>
- Galmarini, S., Koffi, B., Solazzo, E., Keating, T., Hogrefe, C., Schulz, M., et al. (2017). Technical note: Coordination and harmonization of the multi-scale, multi-model activities HTAP2, AQMEII3, and MICS-Asia3: Simulations, emission inventories, boundary conditions, and model output formats. *Atmospheric Chemistry and Physics*, 17(2), 1543–1555. <https://doi.org/10.5194/acp-17-1543-2017>
- Gao, M., Han, Z. W., Tao, Z. N., Li, J. W., Kang, J. E., Huang, K., et al. (2020). Air quality and climate change, Topic 3 of the Model Inter-Comparison Study for Asia Phase III (MICS-Asia III)—Part 2: Aerosol radiative effects and aerosol feedbacks. *Atmospheric Chemistry and Physics*, 20(2), 1147–1161. <https://doi.org/10.5194/acp-20-1147-2020>
- Grell, G. A., & Dévényi, D. (2002). A generalized approach to parameterizing convection combining ensemble and data assimilation techniques. *Geophysical Research Letters*, 29(14), 1693. <https://doi.org/10.1029/2002GL015311>
- Grell, G. A., Peckham, S. E., Schmitz, R., McKeen, S. A., Frost, G., Skamarock, W. C., & Eder, B. (2005). Fully coupled “online” chemistry within the WRF model. *Atmospheric Environment*, 39(37), 6957–6975.
- Guenther, A., Karl, T., Harley, P., Wiedinmyer, C., Palmer, P. I., & Geron, C. (2006). Estimates of global terrestrial isoprene emissions using MEGAN (Model of Emissions of Gases and Aerosols from Nature). *Atmospheric Chemistry and Physics*, 6(11), 3181–3210.
- Guo, H., Sahu, S. K., Kota, S. H., & Zhang, H. L. (2019). Characterization and health risks of criteria air pollutants in Delhi. *Chemosphere*, 225, 27–34. <https://doi.org/10.1016/j.chemosphere.2019.02.154>
- Gupta, P., Remer, L. A., Levy, R. C., & Mattoo, S. (2018). Validation of MODIS 3 km land aerosol optical depth from NASA's EOS Terra and Aqua missions. *Atmospheric Measurement Techniques*, 11(5), 3145–3159.
- Gurney, K. R., Liang, J., O'Keffe, D., Patarasuk, R., Hutchins, M., Huang, J., et al. (2019). Comparison of global downscaled versus bottom-up fossil fuel CO₂ emissions at the urban scale in four US urban areas. *Journal of Geophysical Research: Atmospheres*, 124, 2823–2840. <https://doi.org/10.1029/2018JD028859>
- Han, Z. W., Ueda, H., & An, J. L. (2008). Evaluation and intercomparison of meteorological predictions by five MM5-PBL parameterizations in combination with three land-surface models. *Atmospheric Environment*, 42(2), 233–249. <https://doi.org/10.1016/j.atmosenv.2007.09.053>
- He, Q., Zhang, M., Huang, B., & Tong, X. (2017). MODIS 3 km and 10 km aerosol optical depth for China: Evaluation and comparison. *Atmospheric Environment*, 153, 150–162. <https://doi.org/10.1016/j.atmosenv.2017.01.023>
- Hedelius, J. K., Liu, J., Oda, T., Maksvytov, S., Roehl, C. M., Iraci, L. T., et al. (2018). Southern California megacity CO₂, CH₄, and CO flux estimates using ground- and space-based remote sensing and a Lagrangian model. *Atmospheric Chemistry and Physics*, 18(22), 16271–16291. <https://doi.org/10.5194/acp-18-16271-2018>
- Hitzl, D. E., Chen, Y.-L., & Hsiao, F. (2020). Wintertime easterly and southeasterly airflow in the 'Alenuihāhā channel, Hawaii. *Monthly Weather Review*, 148(4), 1337–1362. <https://doi.org/10.1175/mwr-d-19-0042.1>
- Hong, S. Y., Noh, Y., & Dudhia, J. (2006). A new vertical diffusion package with an explicit treatment of entrainment processes. *Monthly Weather Review*, 134(9), 2318–2341. <https://doi.org/10.1175/Mwr3199.1>
- Horowitz, L. W., Walters, S., Mauzerall, D. L., Emmons, L. K., Rasch, P. J., Granier, C., et al. (2003). A global simulation of tropospheric ozone and related tracers: Description and evaluation of MOZART, version 2. *Journal of Geophysical Research*, 108(D24), 4784. <https://doi.org/10.1029/2002JD002853>
- Hu, J., Li, Y. C., Zhao, T. L., Liu, J., Hu, X.-M., Liu, D. Y., et al. (2018). An important mechanism of regional O₃ transport for summer smog over the Yangtze River Delta in eastern China. *Atmospheric Chemistry and Physics*, 18(22), 16239–16251. <https://doi.org/10.5194/acp-18-16239-2018>
- Hu, J., Wang, Y., Ying, Q., & Zhang, H. (2014). Spatial and temporal variability of PM_{2.5} and PM10 over the North China Plain and the Yangtze River Delta, China. *Atmospheric Environment*, 95, 598–609. <https://doi.org/10.1016/j.atmosenv.2014.07.019>
- Hu, X.-M. (2008). *Incorporation of the model of aerosol dynamics, reaction, ionization, and dissolution (MADRID) into the weather research and forecasting model with chemistry (WRF-Chem): Model development and retrospective applications* (PhD thesis). NC State University. Retrieved from <http://repository.lib.ncsu.edu/ir/handle/1840.16/5241>
- Hu, X.-M. (2015). Boundary layer (atmospheric) and air pollution | Air pollution meteorology. In G. R. North, J. Pyle, & F. Zhang (Eds.), *Encyclopedia of atmospheric sciences* (2nd ed., pp. 227–236). Academic Press.
- Hu, X.-M., Crowell, S., Wang, Q., Zhang, Y., Davis, K. J., Xue, M., et al. (2020). Dynamical downscaling of CO₂ in 2016 over the contiguous United States using WRF-VPRM, a weather-biosphere-online-coupled model. *Journal of Advances in Modeling Earth Systems*, 12, e2019MS001875. <https://doi.org/10.1029/2019MS001875>
- Hu, X.-M., Gourdji, S. M., Davis, K. J., Wang, Q., Zhang, Y., Xue, M., et al. (2021). Implementation of improved parameterization of terrestrial flux in WRF-VPRM improves the simulation of nighttime CO₂ peaks and a daytime CO₂ band ahead of a cold front. *Journal of Geophysical Research: Atmospheres*, <https://doi.org/10.1029/2020jd034362>
- Hu, X.-M., Klein, P. M., & Xue, M. (2013). Evaluation of the updated YSU planetary boundary layer scheme within WRF for wind resource and air quality assessments. *Journal of Geophysical Research: Atmospheres*, 118, 10490–10505. <https://doi.org/10.1002/jgrd.50823>
- Hu, X.-M., Li, X., Xue, M., Wu, D., & Fuentes, J. D. (2016). The formation of barrier winds east of the loess plateau and their effects on dispersion conditions in the north China plains. *Boundary-Layer Meteorology*, 161, 145–163. <https://doi.org/10.1007/s10546-016-0159-4>
- Hu, X.-M., Ma, Z. Q., Lin, W. L., Zhang, H. L., Hu, J. L., Wang, Y., et al. (2014). Impact of the Loess Plateau on the atmospheric boundary layer structure and air quality in the North China Plain: A case study. *Science of the Total Environment*, 499, 228–237. <https://doi.org/10.1016/j.scitotenv.2014.08.053>
- Hu, X.-M., Xue, M., Kong, F. Y., & Zhang, H. L. (2019). Meteorological conditions during an ozone episode in Dallas-Fort Worth, Texas, and impact of their modeling uncertainties on air quality prediction. *Journal of Geophysical Research: Atmospheres*, 124, 1941–1961. <https://doi.org/10.1029/2018JD029791>
- Hu, X.-M., Zhang, Y., Crowell, S., Xue, M., Moore, B., Xiao, X., et al. (2018). *Evaluation of WRF-VPRM CO₂ dynamical downscaling over the Contiguous United States using the ACT-America data*. Paper presented at the 98th annual meeting of American Meteorological Society, Austin. Retrieved from <https://ams.confex.com/ams/98Annual/meetingapp.cgi/Paper/333148>

- Hu, X.-M., Zhang, Y., Jacobson, M. Z., & Chan, C. K. (2008). Coupling and evaluating gas/particle mass transfer treatments for aerosol simulation and forecast. *Journal of Geophysical Research*, 113, D11208. <https://doi.org/10.1029/2007JD009588>
- Huang, X., Ding, A., Wang, Z., Ding, K., Gao, J., Chai, F., & Fu, C. (2020). Amplified transboundary transport of haze by aerosol–boundary layer interaction in China. *Nature Geoscience*, 13(6), 428–434. <https://doi.org/10.1038/s41561-020-0583-4>
- Iacono, M. J., Delamere, J. S., Mlawer, E. J., Shephard, M. W., Clough, S. A., & Collins, W. D. (2008). Radiative forcing by long-lived greenhouse gases: Calculations with the AER radiative transfer models. *Journal of Geophysical Research*, 113, D13103. <https://doi.org/10.1029/2008JD009944>
- Ji, D. S., Li, L., Wang, Y. S., Zhang, J. K., Cheng, M. T., Sun, Y., et al. (2014). The heaviest particulate air-pollution episodes occurred in northern China in January, 2013: Insights gained from observation. *Atmospheric Environment*, 92, 546–556. <https://doi.org/10.1016/j.atmosenv.2014.04.048>
- Jia, R., Luo, M., Liu, Y. Z., Zhu, Q. Z., Hua, S., Wu, C. Q., & Shao, T. B. (2019). Anthropogenic aerosol pollution over the eastern slope of the Tibetan Plateau. *Advances in Atmospheric Sciences*, 36(8), 847–862. <https://doi.org/10.1007/s00376-019-8212-0>
- Kanamitsu, M., Ebisuzaki, W., Woollen, J., Yang, S. K., Hnilo, J. J., Fiorino, M., & Potter, G. L. (2002). NCEP–DOE AMIP-II reanalysis (R-2). *Bulletin of the American Meteorological Society*, 83(11), 1631–1643. <https://doi.org/10.1175/Bams-83-11-1631>
- Kiel, M., O'Dell, C. W., Fisher, B., Eldering, A., Nassar, R., MacDonald, et al. (2019). How bias correction goes wrong: Measurement of X-CO₂ affected by erroneous surface pressure estimates. *Atmospheric Measurement Techniques*, 12(4), 2241–2259. <https://doi.org/10.5194/amt-12-2241-2019>
- Kim, D., Chin, M., Yu, H., Pan, X., Bian, H., Tan, Q., et al. (2019). Asian and trans-Pacific dust: A multimodel and multiremote sensing observation analysis. *Journal of Geophysical Research: Atmospheres*, 124, 13534–13559. <https://doi.org/10.1029/2019JD030822>
- Kong, H., Lin, J. T., Zhang, R. X., Liu, M. Y., Weng, H. J., Ni, R. J., et al. (2019). High-resolution (0.05 degrees x 0.05 degrees) NOx emissions in the Yangtze River Delta inferred from OMI. *Atmospheric Chemistry and Physics*, 19(20), 12835–12856. <https://doi.org/10.5194/acp-19-12835-2019>
- Kong, L., Tang, X., Zhu, J., Wang, Z. F., Fu, J. S., Wang, X. M., et al. (2020). Evaluation and uncertainty investigation of the NO₂, CO and NH₃ modeling over China under the framework of MICS-Asia III. *Atmospheric Chemistry and Physics*, 20(1), 181–202. <https://doi.org/10.5194/acp-20-181-2020>
- Kong, L., Tang, X., Zhu, J., Wang, Z. F., Pan, Y. P., Wu, H. J., et al. (2019). Improved inversion of monthly ammonia emissions in China based on the Chinese ammonia monitoring network and ensemble Kalman filter. *Environmental Science and Technology*, 53(21), 12529–12538. <https://doi.org/10.1021/acs.est.9b02701>
- Konovalov, I. B., Berezin, E. V., Ciais, P., Broquet, G., Beekmann, M., Hadji-Lazaro, J., et al. (2014). Constraining CO₂ emissions from open biomass burning by satellite observations of co-emitted species: A method and its application to wildfires in Siberia. *Atmospheric Chemistry and Physics*, 14(19), 10383–10410. <https://doi.org/10.5194/acp-14-10383-2014>
- Konovalov, I. B., Berezin, E. V., Ciais, P., Broquet, G., Zhuravlev, R. V., & Janssens-Maenhout, G. (2016). Estimation of fossil-fuel CO₂ emissions using satellite measurements of “proxy” species. *Atmospheric Chemistry and Physics*, 16(21), 13509–13540. <https://doi.org/10.5194/acp-16-13509-2016>
- Kopacz, M., Jacob, D. J., Fisher, J. A., Logan, J. A., Zhang, L., Megretskaya, I. A., et al. (2010). Global estimates of CO sources with high resolution by adjoint inversion of multiple satellite datasets (MOPITT, AIRS, SCIAMACHY, TES). *Atmospheric Chemistry and Physics*, 10(3), 855–876. <https://doi.org/10.5194/acp-10-855-2010>
- Krotkov, N. A., McLinden, C. A., Li, C., Lamsal, L. N., Celarier, E. A., Marchenko, S. V., et al. (2016). Aura OMI observations of regional SO₂ and NO₂ pollution changes from 2005 to 2015. *Atmospheric Chemistry and Physics*, 16(7), 4605–4629. <https://doi.org/10.5194/acp-16-4605-2016>
- Kulawik, S. S., Crowell, S., Baker, D., Liu, J., McKain, K., Sweeney, C., et al. (2019). Characterization of OCO-2 and ACOS-GOSAT biases and errors for CO₂ flux estimates. *Atmospheric Measurement Techniques Discussions*, 2019, 1–61. <https://doi.org/10.5194/amt-2019-257>
- Kulawik, S. S., O'Dell, C., Nelson, R. R., & Taylor, T. E. (2019). Validation of OCO-2 error analysis using simulated retrievals. *Atmospheric Measurement Techniques*, 12(10), 5317–5334. <https://doi.org/10.5194/amt-12-5317-2019>
- Lauvaux, T., Miles, N. L., Deng, A. J., Richardson, S. J., Cambaliza, M. O., Davis, K. J., et al. (2016). High-resolution atmospheric inversion of urban CO₂ emissions during the dormant season of the Indianapolis Flux Experiment (INFLUX). *Journal of Geophysical Research: Atmospheres*, 121, 5213–5236. <https://doi.org/10.1002/2015JD024473>
- Leibensperger, E. M., Mickley, L. J., & Jacob, D. J. (2008). Sensitivity of US air quality to mid-latitude cyclone frequency and implications of 1980–2006 climate change. *Atmospheric Chemistry and Physics*, 8(23), 7075–7086.
- Leibensperger, E. M., Mickley, L. J., Jacob, D. J., & Barrett, S. R. H. (2011). Intercontinental influence of NOx and CO emissions on particulate matter air quality. *Atmospheric Environment*, 45(19), 3318–3324. <https://doi.org/10.1016/j.atmosenv.2011.02.023>
- Li, C., McLinden, C., Fioletov, V., Krotkov, N., Carn, S., Joiner, J., et al. (2017). India is overtaking China as the World's largest emitter of anthropogenic sulfur dioxide. *Scientific Reports*, 7, 14304. <https://doi.org/10.1038/s41598-017-14639-8>
- Li, J., Nagashima, T., Kong, L., Ge, B. Z., Yamaji, K., Fu, J. S., et al. (2019). Model evaluation and intercomparison of surface-level ozone and relevant species in East Asia in the context of MICS-Asia Phase III—Part 1: Overview. *Atmospheric Chemistry and Physics*, 19(20), 12993–13015. <https://doi.org/10.5194/acp-19-12993-2019>
- Li, M. M., Wang, T. J., Xie, M., Li, S., Zhuang, B. L., Huang, X., et al. (2019). Formation and evolution mechanisms for two extreme haze episodes in the Yangtze River Delta Region of China during winter 2016. *Journal of Geophysical Research: Atmospheres*, 124, 3607–3623. <https://doi.org/10.1029/2019JD030535>
- Li, T. Y., Deng, X. J., Li, Y., Song, Y. S., Li, L. Y., Tan, H. B., & Wang, C. L. (2018). Transport paths and vertical exchange characteristics of haze pollution in Southern China. *Science of the Total Environment*, 625, 1074–1087. <https://doi.org/10.1016/j.scitotenv.2017.12.235>
- Li, X., Hu, X.-M., Cai, C., Jia, Q., Zhang, Y., Liu, J., et al. (2020). Terrestrial CO₂ fluxes, concentrations, sources and budget in northeast China: Observational and modeling studies. *Journal of Geophysical Research: Atmospheres*, 125, e2019JD031686. <https://doi.org/10.1029/2019JD031686>
- Li, X. L., Hu, X.-M., Ma, Y. J., Wang, Y. F., Li, L. G., & Zhao, Z. Q. (2019). Impact of planetary boundary layer structure on the formation and evolution of air-pollution episodes in Shenyang, Northeast China. *Atmospheric Environment*, 214, 116850. <https://doi.org/10.1016/j.atmosenv.2019.116850>
- Li, X. L., Hu, X.-M., Shi, S. Y., Shen, L. D., Luan, L., & Ma, Y. J. (2019). Spatiotemporal variations and regional transport of air pollutants in two urban agglomerations in Northeast China Plain. *Chinese Geographical Science*, 29(6), 917–933. <https://doi.org/10.1007/s11769-019-1081-8>
- Liao, X., Tu, H., Maddock, J. E., Fan, S., Lan, G. L., Wu, Y. Y., et al. (2015). Residents' perception of air quality, pollution sources, and air pollution control in Nanchang, China. *Atmospheric Pollution Research*, 6(5), 835–841. <https://doi.org/10.5094/apr.2015.092>

- Lin, N., Wang, Y. X., Zhang, Y., & Yang, K. (2019). A large decline of tropospheric NO₂ in China observed from space by SNPP OMPS. *Science of the Total Environment*, 675, 337–342. <https://doi.org/10.1016/j.scitotenv.2019.04.090>
- Lindenmaier, R., Dubey, M. K., Henderson, B. G., Butterfield, Z. T., Herman, J. R., Rahn, T., & Lee, S. H. (2014). Multiscale observations of CO₂, (CO₂)-C-13, and pollutants at four corners for emission verification and attribution. *Proceedings of the National Academy of Sciences of the United States of America*, 111(23), 8386–8391. <https://doi.org/10.1073/pnas.1321883111>
- Liu, P., Hogrefe, C., Im, U., Christensen, J. H., Bieser, J., Nopmongcol, U., et al. (2018). Attributing differences in the fate of lateral boundary ozone in AQMEII3 models to physical process representations. *Atmospheric Chemistry and Physics*, 18(23), 17157–17175. <https://doi.org/10.5194/acp-18-17157-2018>
- Liu, Q., Sheng, L., Cao, Z., Diao, Y., Wang, W., & Zhou, Y. (2017). Dual effects of the winter monsoon on haze-fog variations in eastern China. *Journal of Geophysical Research: Atmospheres*, 122, 5857–5869. <https://doi.org/10.1002/2016JD026296>
- Lopez, M., Schmidt, M., Delmotte, M., Colomb, A., Gros, V., Janssen, C., et al. (2013). CO, NOx and 13CO₂ as tracers for fossil fuel CO₂: Results from a pilot study in Paris during winter 2010. *Atmospheric Chemistry and Physics*, 13(15), 7343–7358. <https://doi.org/10.5194/acp-13-7343-2013>
- Lowry, D., Lanoiselle, M. E., Fisher, R. E., Martin, M., Fowler, C. M. R., France, J. L., et al. (2016). Marked long-term decline in ambient CO mixing ratio in SE England, 1997–2014: Evidence of policy success in improving air quality. *Scientific Reports*, 6(12). <https://doi.org/10.1038/srep25661>
- Lu, L. J., Chen, B. Z., Guo, L. F., Zhang, H. F., & Li, Y. P. (2019). A regional data assimilation system for estimating CO surface flux from atmospheric mixing ratio observations—A case study of Xuzhou, China. *Environmental Science and Pollution Research*, 26(9), 8748–8757. <https://doi.org/10.1007/s11356-019-04246-7>
- Ma, S., Zhang, X., Gao, C., Tong, D. Q., Xiu, A., Wu, G., et al. (2019). Multimodel simulations of a springtime dust storm over northeastern China: Implications of an evaluation of four commonly used air quality models (CMAQ v5.2.1, CAMx v6.50, CHIMERE v2017r4, and WRF-Chem v3.9.1). *Geoscientific Model Development*, 12(11), 4603–4625. <https://doi.org/10.5194/gmd-12-4603-2019>
- Ma, Z. W., Hu, X. F., Sayer, A. M., Levy, R., Zhang, Q., Xue, Y. G., et al. (2016). Satellite-based spatiotemporal trends in PM2.5 concentrations: China, 2004–2013. *Environmental Health Perspectives*, 124(2), 184–192. <https://doi.org/10.1289/ehp.1409481>
- Mahadevan, P., Wofsy, S. C., Matross, D. M., Xiao, X. M., Dunn, A. L., Lin, J. C., et al. (2008). A satellite-based biosphere parameterization for net ecosystem CO₂ exchange: Vegetation Photosynthesis and Respiration Model (VPRM). *Global Biogeochemical Cycles*, 22, GB2005. <https://doi.org/10.1029/2006gb002735>
- Martin, C. R., Zeng, N., Karion, A., Mueller, K., Ghosh, S., Lopez-Coto, I., et al. (2019). Investigating sources of variability and error in simulations of carbon dioxide in an urban region. *Atmospheric Environment*, 199, 55–69. <https://doi.org/10.1016/j.atmosenv.2018.11.013>
- Matthias, V. (2008). The aerosol distribution in Europe derived with the Community Multiscale Air Quality (CMAQ) model: Comparison to near surface in situ and sun photometer measurements. *Atmospheric Chemistry and Physics*, 8(17), 5077–5097. <https://doi.org/10.5194/acp-8-5077-2008>
- Miao, Y., Hu, X.-M., Liu, S., Qian, T., Xue, M., Zheng, Y., & Wang, S. (2015). Seasonal variation of local atmospheric circulations and boundary layer structure in the Beijing-Tianjin-Hebei region and implications for air quality. *Journal of Advances in Modeling Earth Systems*, 7(4), 1602–1626. <https://doi.org/10.1002/2015MS000522>
- Miao, Y., & Liu, S. (2019). Linkages between aerosol pollution and planetary boundary layer structure in China. *Science of the Total Environment*, 650, 288–296. <https://doi.org/10.1016/j.scitotenv.2018.09.032>
- Mlawer, E. J., Taubman, S. J., Brown, P. D., Iacono, M. J., & Clough, S. A. (1997). Radiative transfer for inhomogeneous atmospheres: RRTM, a validated correlated-k model for the longwave. *Journal of Geophysical Research*, 102(D14), 16663–16682. <https://doi.org/10.1029/97JD00237>
- Morrison, H., Thompson, G., & Tatarki, V. (2009). Impact of cloud microphysics on the development of trailing stratiform precipitation in a simulated squall line: Comparison of one- and two-moment schemes. *Monthly Weather Review*, 137(3), 991–1007. <https://doi.org/10.1175/2008mwr2556.1>
- Munchak, L. A., Levy, R. C., Mattoo, S., Remer, L. A., Holben, B. N., Schafer, J. S., et al. (2013). MODIS 3 km aerosol product: Applications over land in an urban/suburban region. *Atmospheric Measurement Techniques*, 6(7), 1747–1759. <https://doi.org/10.5194/amt-6-1747-2013>
- Nassar, R., Hill, T. G., McLinden, C. A., Wunch, D., Jones, D. B. A., & Crisp, D. (2017). Quantifying CO₂ emissions from individual power plants from space. *Geophysical Research Letters*, 44, 10045–10053. <https://doi.org/10.1002/2017GL074702>
- Ning, G. C., Yim, S. H. L., Wang, S. G., Duan, B. L., Nie, C. Q., Yang, X., et al. (2019). Synergistic effects of synoptic weather patterns and topography on air quality: A case of the Sichuan Basin of China. *Climate Dynamics*, 53(11), 6729–6744. <https://doi.org/10.1007/s00382-019-04954-3>
- Oda, T., Bun, R., Kinakh, V., Topylko, P., Halushchak, M., Marland, G., et al. (2019). Errors and uncertainties in a gridded carbon dioxide emissions inventory. *Mitigation and Adaptation Strategies for Global Change*, 24(6), 1007–1050. <https://doi.org/10.1007/s11027-019-09877-2>
- Oda, T., Lauvax, T., Lu, D. S., Rao, P., Miles, N. L., Richardson, S. J., & Gurney, K. R. (2017). On the impact of granularity of space-based urban CO₂ emissions in urban atmospheric inversions: A case study for Indianapolis. *Elementa-Science of the Anthropocene*, 5, 28. <https://doi.org/10.1525/elementa.146>
- Oda, T., Maksyutov, S., & Andres, R. J. (2018). The Open-source Data Inventory for Anthropogenic CO₂, version 2016 (ODIAC2016): A global monthly fossil fuel CO₂ gridded emissions data product for tracer transport simulations and surface flux inversions. *Earth System Science Data*, 10(1), 87–107. <https://doi.org/10.5194/essd-10-87-2018>
- O'Dell, C. W., Eldering, A., Wennberg, P. O., Crisp, D., Gunson, M. R., Fisher, B., et al. (2018). Improved retrievals of carbon dioxide from Orbiting Carbon Observatory-2 with the version 8 ACOS algorithm. *Atmospheric Measurement Techniques*, 11(12), 6539–6576. <https://doi.org/10.5194/amt-11-6539-2018>
- Overland, J. E., & Walter, B. A. (1981). Gap winds in the strait of Juan De Fuca. *Monthly Weather Review*, 109(10), 2221–2233. [https://doi.org/10.1175/1520-0493\(1981\)109<2221:Gwts>2.0.Co;2](https://doi.org/10.1175/1520-0493(1981)109<2221:Gwts>2.0.Co;2)
- Palmer, P. I., Suntharalingam, P., Jones, D. B. A., Jacob, D. J., Streets, D. G., Fu, Q. Y., et al. (2006). Using CO₂: CO correlations to improve inverse analyses of carbon fluxes. *Journal of Geophysical Research*, 111, D12318. <https://doi.org/10.1029/2005JD006697>
- Pere, J. C., Mallet, M., Pont, V., & Bessagnet, B. (2010). Evaluation of an aerosol optical scheme in the chemistry-transport model CHIMERE. *Atmospheric Environment*, 44(30), 3688–3699. <https://doi.org/10.1016/j.atmosenv.2010.06.034>
- Peters, W., Jacobson, A. R., Sweeney, C., Andrews, A. E., Conway, T. J., Masarie, K., et al. (2007). An atmospheric perspective on North American carbon dioxide exchange: CarbonTracker. *Proceedings of the National Academy of Sciences of the United States of America*, 104(48), 18925–18930. <https://doi.org/10.1073/pnas.0708986104>

- Remer, L. A., Mattoo, S., Levy, R. C., & Munchak, L. A. (2013). MODIS 3 km aerosol product: Algorithm and global perspective. *Atmospheric Measurement Techniques*, 6(7), 1829–1844. <https://doi.org/10.5194/amt-6-1829-2013>
- Reuter, M., Buchwitz, M., Schneising, O., Krautwurst, S., O'Dell, C. W., Richter, A., et al. (2019). Towards monitoring localized CO₂ emissions from space: Co-located regional CO₂ and NO₂ enhancements observed by the OCO-2 and S5P satellites. *Atmospheric Chemistry and Physics*, 19(14), 9371–9383. <https://doi.org/10.5194/acp-19-9371-2019>
- Roy, B., Mathur, R., Gilliland, A. B., & Howard, S. C. (2007). A comparison of CMAQ-based aerosol properties with IMPROVE, MODIS, and AERONET data. *Journal of Geophysical Research*, 112, D14301. <https://doi.org/10.1029/2006JD008085>
- Russell, A. (1997). Regional photochemical air quality modeling: Model formulations, history, and state of the science. *Annual Review of Energy and the Environment*, 22, 537–588. <https://doi.org/10.1146/annurev.energy.22.1.537>
- Schell, B., Ackermann, I. J., Hass, H., Binkowski, F. S., & Ebel, A. (2001). Modeling the formation of secondary organic aerosol within a comprehensive air quality model system. *Journal of Geophysical Research*, 106(D22), 28275–28293. <https://doi.org/10.1029/2001JD000384>
- Seigneur, C., Pun, B., Pai, P., Louis, J. F., Solomon, P., Emery, C., et al. (2000). Guidance for the performance evaluation of three-dimensional air quality modeling systems for particulate matter and visibility. *Journal of the Air & Waste Management Association*, 50(4), 588–599.
- Shim, C., Han, J., Henze, D. K., & Yoon, T. (2019). Identifying local anthropogenic CO₂ emissions with satellite retrievals: A case study in South Korea. *International Journal of Remote Sensing*, 40(3), 1011–1029. <https://doi.org/10.1080/01431161.2018.1523585>
- Silva, S. J., & Arellano, A. F. (2017). Characterizing regional-scale combustion using satellite retrievals of CO, NO₂ and CO₂. *Remote Sensing*, 9(7), 744. <https://doi.org/10.3390/rs9070744>
- Skamarock, W. C., & Klemp, J. B. (2008). A time-split nonhydrostatic atmospheric model for weather research and forecasting applications. *Journal of Computational Physics*, 227(7), 3465–3485. <https://doi.org/10.1016/j.jcp.2007.01.037>
- Sokhi, R. S., Mao, H., Srimath, S. T. G., Fan, S., Kitwiroom, N., Luhana, L., et al. (2008). An integrated multi-model approach for air quality assessment: Development and evaluation of the OSCAR Air Quality Assessment System. *Environmental Modelling and Software*, 23(3), 268–281. <https://doi.org/10.1016/j.envsoft.2007.03.006>
- Solazzo, E., Bianconi, R., Hogrefe, C., Curci, G., Tuccella, P., Alyuz, U., et al. (2017). Evaluation and error apportionment of an ensemble of atmospheric chemistry transport modeling systems: Multivariable temporal and spatial breakdown. *Atmospheric Chemistry and Physics*, 17(4), 3001–3054. <https://doi.org/10.5194/acp-17-3001-2017>
- Sun, P., Nie, W., Wang, T., Chi, X., Huang, X., Xu, Z., et al. (2020). Impact of air transport and secondary formation on haze pollution in the Yangtze River Delta: In situ online observations in Shanghai and Nanjing. *Atmospheric Environment*, 225, 117350. <https://doi.org/10.1016/j.atmosenv.2020.117350>
- Sun, Y. L., Wang, Z. F., Du, W., Zhang, Q., Wang, Q. Q., Fu, P. Q., et al. (2015). Long-term real-time measurements of aerosol particle composition in Beijing, China: Seasonal variations, meteorological effects, and source analysis. *Atmospheric Chemistry and Physics*, 15(17), 10149–10165. <https://doi.org/10.5194/acp-15-10149-2015>
- Susskind, J., Barnet, C. D., & Blaisdell, J. M. (2003). Retrieval of atmospheric and surface parameters from AIRS/AMSU/HSB data in the presence of clouds. *IEEE Transactions on Geoscience and Remote Sensing*, 41(2), 390–409.
- Tai, A. P. K., Mickley, L. J., & Jacob, D. J. (2012). Impact of 2000–2050 climate change on fine particulate matter (PM2.5) air quality inferred from a multi-model analysis of meteorological modes. *Atmospheric Chemistry and Physics*, 12(23), 11329–11337. <https://doi.org/10.5194/acp-12-11329-2012>
- Takahashi, T., Sutherland, S. C., Wanninkhof, R., Sweeney, C., Feely, R. A., Chipman, D. W., et al. (2009). Climatological mean and decadal change in surface ocean pCO₂, and net sea-air CO₂ flux over the global oceans. *Deep-Sea Research Part II-Topical Studies in Oceanography*, 56(8–10), 554–577.
- Tang, W., Arellano, A. F., Gaubert, B., Miyazaki, K., & Worden, H. M. (2019). Satellite data reveal a common combustion emission pathway for major cities in China. *Atmospheric Chemistry and Physics*, 19(7), 4269–4288. <https://doi.org/10.5194/acp-19-4269-2019>
- Tewari, M., Chen, F., Wang, W., Dudhia, J., Lemone, M. A., Mitchell, K., et al. (2004). Implementation and verification of the unified NOAH land surface model in the WRF model. Paper presented at the Conference on Weather Analysis and Forecasting/Conference on Numerical Weather Prediction.
- Thomas, A., Huff, A. K., Hu, X. M., & Zhang, F. (2019). Quantifying uncertainties of ground-level ozone within WRF-Chem simulations in the mid-Atlantic region of the United States as a response to variability. *Journal of Advances in Modeling Earth Systems*, 11(4), 1100–1116. <https://doi.org/10.1029/2018ms001457>
- Turnbull, J. C., Karion, A., Fischer, M. L., Faloona, I., Guilderson, T., Lehman, S. J., et al. (2011). Assessment of fossil fuel carbon dioxide and other anthropogenic trace gas emissions from airborne measurements over Sacramento, California in spring 2009. *Atmospheric Chemistry and Physics*, 11(2), 705–721. <https://doi.org/10.5194/acp-11-705-2011>
- Wang, H., Jacob, D. J., Kopacz, M., Jones, D. B. A., Suntharalingam, P., Fisher, J. A., et al. (2009). Error correlation between CO₂ and CO as constraint for CO₂ flux inversions using satellite data. *Atmospheric Chemistry and Physics*, 9(19), 7313–7323. <https://doi.org/10.5194/acp-9-7313-2009>
- Wang, L. T., Wei, Z., Yang, J., Zhang, Y., Zhang, F. F., Su, J., et al. (2014). The 2013 severe haze over southern Hebei, China: Model evaluation, source apportionment, and policy implications. *Atmospheric Chemistry and Physics*, 14(6), 3151–3173. <https://doi.org/10.5194/acp-14-3151-2014>
- Wang, S. X., & Hao, J. M. (2012). Air quality management in China: Issues, challenges, and options. *Journal of Environmental Sciences-China*, 24(1), 2–13. [https://doi.org/10.1016/s1001-0742\(11\)60724-9](https://doi.org/10.1016/s1001-0742(11)60724-9)
- Wang, Z. F., Li, J., Wang, Z., Yang, W. Y., Tang, X., Ge, B. Z., et al. (2014). Modeling study of regional severe hazes over mid-eastern China in January 2013 and its implications on pollution prevention and control. *Science China Earth Sciences*, 57(1), 3–13. <https://doi.org/10.1007/s11430-013-4793-0>
- Warner, J., Comer, M. M., Barnet, C. D., McMillan, W. W., Wolf, W., Maddy, E., & Sachse, G. (2007). A comparison of satellite tropospheric carbon monoxide measurements from AIRS and MOPITT during INTEX-A. *Journal of Geophysical Research*, 112, D12S17. <https://doi.org/10.1029/2006JD007925>
- Wei, J., Li, Z. Q., Guo, J. P., Sun, L., Huang, W., Xue, W. H., et al. (2019). Satellite-derived 1-km-resolution PM1 concentrations from 2014 to 2018 across China. *Environmental Science and Technology*, 53(22), 13265–13274. <https://doi.org/10.1021/acs.est.9b03258>
- Worden, H. M., Deeter, M. N., Frankenberg, C., George, M., Nicithiu, F., Worden, J., et al. (2013). Decadal record of satellite carbon monoxide observations. *Atmospheric Chemistry and Physics*, 13(2), 837–850. <https://doi.org/10.5194/acp-13-837-2013>
- Wu, D., Lin, J. C., Fasoli, B., Oda, T., Ye, X. X., Lauvaux, T., & Kort, E. A. (2018). A Lagrangian approach towards extracting signals of urban CO₂ emissions from satellite observations of atmospheric column CO₂ (XCO₂): X-Stochastic Time-Inverted Lagrangian Transport model (“X-STILT v1”). *Geoscientific Model Development*, 11(12), 4843–4871. <https://doi.org/10.5194/gmd-11-4843-2018>

- Wu, D., Lin, J. C., Oda, T., & Kort, E. A. (2020). Space-based quantification of per capita CO₂ emissions from cities. *Environmental Research Letters*, 15(3), 035004. <https://doi.org/10.1088/1748-9326/ab68eb>
- Wunch, D., Wennberg, P. O., Osterman, G., Fisher, B., Naylor, B., Roehl, C. M., et al. (2017). Comparisons of the Orbiting Carbon Observatory-2 (OCO-2) X-CO₂ measurements with TCCON. *Atmospheric Measurement Techniques*, 10(6), 2209–2238. <https://doi.org/10.5194/amt-10-2209-2017>
- Wunch, D., Wennberg, P. O., Toon, G. C., Keppel-Aleks, G., & Yavin, Y. G. (2009). Emissions of greenhouse gases from a North American megacity. *Geophysical Research Letters*, 36, L15810. <https://doi.org/10.1029/2009GL039825>
- Xiao, X. M., Hollinger, D., Aber, J., Goltz, M., Davidson, E. A., Zhang, Q. Y., & Moore, B. (2004). Satellite-based modeling of gross primary production in an evergreen needleleaf forest. *Remote Sensing of Environment*, 89(4), 519–534. <https://doi.org/10.1016/j.rse.2003.11.008>
- Xiao, Z., Miao, Y., Du, X., Tang, W., Yu, Y., Zhang, X., & Che, H. (2020). Impacts of regional transport and boundary layer structure on the PM2.5 pollution in Wuhan, Central China. *Atmospheric Environment*, 230, 117508. <https://doi.org/10.1016/j.atmosenv.2020.117508>
- Xie, G. Q., Wang, M., Pan, J., & Zhu, Y. (2019). Spatio-temporal variations and trends of MODIS C6.1 Dark Target and Deep Blue merged aerosol optical depth over China during 2000–2017. *Atmospheric Environment*, 214, 11. <https://doi.org/10.1016/j.atmosenv.2019.116846>
- Xu, J., Han, F., Li, M. Z., Zhang, Z. Z., Du, X. H., & Wei, P. (2019). On the opposite seasonality of MODIS AOD and surface PM2.5 over the Northern China plain. *Atmospheric Environment*, 215, 9. <https://doi.org/10.1016/j.atmosenv.2019.116909>
- Xu, J., Tie, X., Gao, W., Lin, Y., & Fu, Q. (2019). Measurement and model analyses of the ozone variation during 2006 to 2015 and its response to emission change in megacity Shanghai, China. *Atmospheric Chemistry and Physics*, 19(14), 9017–9035. <https://doi.org/10.5194/acp-19-9017-2019>
- Yang, H. O., Chen, W. B., & Liang, Z. F. (2017). Impact of land use on PM2.5 pollution in a representative city of middle China. *International Journal of Environmental Research and Public Health*, 14(5), 14. <https://doi.org/10.3390/ijerph14050462>
- Yang, K., Carn, S. A., Ge, C., Wang, J., & Dickerson, R. R. (2014). Advancing measurements of tropospheric NO₂ from space: New algorithm and first global results from OMPS. *Geophysical Research Letters*, 41, 4777–4786. <https://doi.org/10.1002/2014GL060136>
- Yang, K., Dickerson, R. R., Carn, S. A., Ge, C., & Wang, J. (2013). First observations of SO₂ from the satellite Suomi NPP OMPS: Widespread air pollution events over China. *Geophysical Research Letters*, 40, 4957–4962. <https://doi.org/10.1002/grl.50952>
- Yang, S., Duan, F., Ma, Y., He, K., Zhu, L., Ma, T., et al. (2019). Haze formation indicator based on observation of critical carbonaceous species in the atmosphere. *Environmental Pollution*, 244, 84–92. <https://doi.org/10.1016/j.envpol.2018.10.006>
- Ye, X., Lauvaux, T., Kort, E. A., Oda, T., Feng, S., Lin, J. C., et al. (2020). Constraining fossil fuel CO₂ emissions from urban area using OCO-2 observations of total column CO₂. *Journal of Geophysical Research: Atmospheres*, 125, e2019JD030528. <https://doi.org/10.1029/2019JD030528>
- Yokota, T., Yoshida, Y., Eguchi, N., Ota, Y., Tanaka, T., Watanabe, H., & Maksyutov, S. (2009). Global concentrations of CO₂ and CH₄ retrieved from GOSAT: First preliminary results. *SOLA*, 5, 160–163. <https://doi.org/10.2151/sola.2009-041>
- Yu, C., Zhao, T., Bai, Y., Zhang, L., Kong, S., Yu, X., et al. (2020). Heavy air pollution with a unique “non-stagnant” atmospheric boundary layer in the Yangtze River middle basin aggravated by regional transport of PM2.5 over China. *Atmospheric Chemistry and Physics*, 20(12), 7217–7230. <https://doi.org/10.5194/acp-20-7217-2020>
- Yu, H., Remer, L. A., Chin, M., Bian, H., Kleidman, R. G., & Diehl, T. (2008). A satellite-based assessment of transpacific transport of pollution aerosol. *Journal of Geophysical Research*, 113, D14S12. <https://doi.org/10.1029/2007JD009349>
- Yu, S. C., Eder, B., Dennis, R., Chu, S. H., & Schwartz, S. E. (2006). New unbiased symmetric metrics for evaluation of air quality models. *Atmospheric Science Letters*, 7(1), 26–34. <https://doi.org/10.1002/asl.125>
- Yurganov, L. N., McMillan, W. W., Dzhola, A. V., Grechko, E. I., Jones, N. B., & van der Werf, G. R. (2008). Global AIRS and MOPITT CO measurements: Validation, comparison, and links to biomass burning variations and carbon cycle. *Journal of Geophysical Research*, 113, D09301. <https://doi.org/10.1029/2007JD009229>
- Zhang, H., Chen, G., Hu, J., Chen, S.-H., Wiedinmyer, C., Kleeman, M., & Ying, Q. (2014). Evaluation of a seven-year air quality simulation using the Weather Research and Forecasting (WRF)/Community Multiscale Air Quality (CMAQ) models in the eastern United States. *Science of the Total Environment*, 473–474, 275–285. <https://doi.org/10.1016/j.scitotenv.2013.11.121>
- Zhang, H., Wang, Y., Hu, J., Ying, Q., & Hu, X.-M. (2015). Relationships between meteorological parameters and criteria air pollutants in three megalopolises in China. *Environmental Research*, 140, 242–254. <https://doi.org/10.1016/j.envres.2015.04.004>
- Zhang, L., Jacob, D. J., Liu, X., Logan, J. A., Chance, K., Eldering, A., & Bojkov, B. R. (2010). Intercomparison methods for satellite measurements of atmospheric composition: Application to tropospheric ozone from TES and OMI. *Atmospheric Chemistry and Physics*, 10(10), 4725–4739. <https://doi.org/10.5194/acp-10-4725-2010>
- Zhang, L., Zhao, T., Gong, S., Kong, S., Tang, L., Liu, D., et al. (2018). Updated emission inventories of power plants in simulating air quality during haze periods over East China. *Atmospheric Chemistry and Physics*, 18(3), 2065–2079. <https://doi.org/10.5194/acp-18-2065-2018>
- Zhang, L. J., Yuan, Z. K., Maddock, J. E., Zhang, P., Jiang, Z. Q., Lee, T., et al. (2014). Air quality and environmental protection concerns among residents in Nanchang, China. *Air Quality Atmosphere and Health*, 7(4), 441–448. <https://doi.org/10.1007/s11869-014-0255-x>
- Zhang, Y., Chen, Y.-L., & Kodama, K. (2005). Validation of the coupled NCEP mesoscale spectral model and an advanced land surface model over the Hawaiian Islands. Part II: A high wind event. *Weather and Forecasting*, 20(6), 873–895. <https://doi.org/10.1175/waf892.1>
- Zhao, X. F., Zhao, Y., Chen, D., Li, C. Y., & Zhang, J. (2019). Top-down estimate of black carbon emissions for city clusters using ground observations: A case study in southern Jiangsu, China. *Atmospheric Chemistry and Physics*, 19(4), 2095–2113. <https://doi.org/10.5194/acp-19-2095-2019>
- Zhao, Y., Yu, R. L., Hu, G. R., Lin, X. H., & Liu, X. R. (2017). Chemical characteristics and Pb isotopic compositions of PM2.5 in Nanchang, China. *Particuology*, 32, 95–102. <https://doi.org/10.1016/j.partic.2016.07.009>
- Zhou, Y., Luo, B., Li, J., Hao, Y. F., Yang, W. W., Shi, F. T., et al. (2019). Characteristics of six criteria air pollutants before, during, and after a severe air pollution episode caused by biomass burning in the southern Sichuan Basin, China. *Atmospheric Environment*, 215, 116840. <https://doi.org/10.1016/j.atmosenv.2019.116840>